

THE UNIVERSITY OF CALGARY

Measurement of beat length in high
birefringent fibers using Faraday
magneto-optic effect

by

Muhammad Raziullah Khan

A THESIS

SUBMITTED TO THE FACULTY OF GRADUATE STUDIES

IN PARTIAL FULFILMENT OF THE REQUIREMENTS FOR

THE DEGREE OF MASTER OF SCIENCE

DEPARTMENT OF ELECTRICAL AND COMPUTER ENGINEERING

CALGARY, ALBERTA

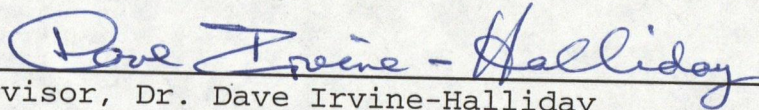
June, 1996

© Muhammad R. Khan 1996

THE UNIVERSITY OF CALGARY

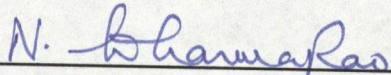
FACULTY OF GRADUATE STUDIES

The undersigned certify that they have read, and recommend to the Faculty of graduate studies for acceptance, a thesis entitled, "Measurement of beat length in High Birefringent fibers using Faraday magneto-optic effect", submitted by Muhammad R. Khan in partial fulfilment of the requirements for the degree of Master of Science.



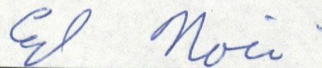
Supervisor, Dr. Dave Irvine-Halliday

Department of Electrical and Computer Engineering



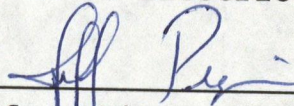
Dr. N. Dharma Rao

Department of Electrical and Computer Engineering



Dr. Edwin P. Nowicki

Department of Electrical and Computer Engineering



Dr. Jeffrey Pieper

Department of Mechanical Engineering

Date: 10 June 96

Abstract

The polarization maintaining capability of birefringent optical fibers can be described in terms of their modal birefringence or beat length. Beat length is the minimum length of fiber over which the state of polarization (SOP) returns to its original value, that is, after one cycle. Since existing techniques for beat length measurement have a number of significant limitations in measuring small beat lengths, a technique to measure beat length in High Birefringent (Hi-Bi) fibers using the Faraday magneto-optic effect is proposed.

Step by step design and development procedures for implementing the proposed technique, including the experimental set-up, are described. Experimental measurements have been carried out and the beat lengths of four fibers measured successfully. The experimental results are very close to the beat lengths specified by the manufacturers and this technique can be used to measure the beat length non-destructively in contrast to some existing techniques.

The experimental challenges and their solutions, as described in this thesis, will be helpful in the future design of a prototype beat length measurement instrument. The experimental results indicate that this relatively simple and economical beat length measurement technique is a legitimate

candidate to replace existing instruments used for this purpose.

Definitions

Bandwidth: The capacity of an optical fiber to transmit information (often expressed in megabits/sec.km).

Birefringence: The separation of a light beam, as it penetrates a doubly refracting object, into two diverging beams, commonly known as ordinary and extra-ordinary beams.

Cross-talk: The undesired coupling of energy between independent signals travelling in a waveguide.

Cutoff wavelength: The wavelength at which a particular waveguide mode ceases to be bound to the waveguide and becomes a radiation mode.

Fiber optics: The branch of technology concerned with the transmission of optical power through fibers made of transparent materials such as glass, fused silica, or plastic.

Linearly polarized: A beam is said to be linearly polarized if a single electric field vector perpendicular to the direction of propagation can represent the beam.

Mode field diameter: A practical representation of the extent of the energy-carrying region of the fiber core and cladding.

Optically active: When a beam of linearly polarized light passes through certain substances such as quartz it will emerge still linearly polarized but rotated by some fixed angle. These substances are said to be optically active, and the rotation of the electric field vector is referred to as

natural rotation.

Polarization-Maintaining (PM) fiber: These fibers are designed to ensure that with a linearly polarized input signal, having a particular spatial orientation of polarization, the light wave emerging from a long fiber will be essentially linearly polarized at the same state of polarization as the input signal.

Single-mode fiber: An optical waveguide through which only one mode will propagate.

State of Polarization (SOP): The SOP of an electro-magnetic wave is characterized by the orientation of the electric field vector representing the propagating wave along a transmission path. There are three possible states of polarization, elliptical, circular and linear. The later two are degenerative cases of elliptical polarization.

Verdet constant: It is defined as the rotation per unit path per unit field strength of the electric vector.

Acknowledgement

I would like to express my sincere gratitude to my distinguished supervisor, Dr. Dave Irvine-Halliday, for his constant guidance, encouragement, understanding and academic and financial support throughout the whole program. His valuable suggestions and criticism from time to time enabled me to present my research and this thesis in this form.

I would like to thank the learned professors and support staff in the Department of Electrical and Computer Engineering, the University of Calgary, for their invaluable help during my study. I am also thankful to NSERC for its financial support of this project.

Grateful acknowledgement are extended to Dr. Jim Gleeson of the University of Calgary Physics Department; Dr. Mike Messerly of 3M Inc; Dave Clegg of TR Labs, Edmonton; Peng-Gang Zhang of Mark-4 Inc; my friends particularly Insram and Jawed, fellow students and many other people around me, whose names are impossible to be listed here, for their valuable help.

I am indebted to my wife Azra who is always understanding, patient and encouraging and without her constant support I could not have finished this program. I also thank my beloved children, Malika, Saleha and Wasi as their charming faces and sweet talk supported me during my many hard days.

Dedication

To my parents!

Table of contents

Abstract	iii
Definitions	v
Acknowledgments	vii
Dedication	viii
List of Figures	xii
List of Tables	xvi
List of Symbols	xvii
1. Introduction	1
1.1 Introduction	1
1.2 Literature review	3
1.3 Thesis outline	5
2. Optics	6
2.1 Light	6
2.2 Polarized light	7
2.3 Mathematics of polarized light	10
2.4 Birefringence	13
2.5 Polarization maintaining (PM) fibers	14
2.6 Lo-Bi and Hi-Bi PM fibers	16
2.7 Optical system components	17
2.7.1 Lenses	18
2.7.2 Retarder (Quarter-wave plate)	19
2.7.3 Glan-Thompson polarizer	20
2.7.4 Prism (Wollaston)	21
2.7.5 Electro-optical components	22

2.7.6	Mechanical components	24
3.	Magnetics	26
3.1	Magnetics	26
3.1.1	History	26
3.1.2	Electro-magnetics	27
3.2	Magnetic cores	31
3.2.1	Magnetic materials	31
3.2.2	Magnetic cores	32
4.	Faraday Magneto-optic effect	36
5.	Beat length measurement technique	40
5.1	Basic principle	40
5.2	Mathematics of the technique	41
5.3	Implementation scheme	48
6.	Instrument Design	50
6.1	Basic requirements	50
6.2	Coupling the power into the fiber	50
6.3	Magnetic head design	53
6.4	Signal processing unit	58
6.5	Assembling the instrument	65
7.	Observations and results.....	67
7.1	Experimental procedure and initial results	68
7.2	Sources of error and their corrections	75
7.3	Intermediate results	78
7.4	Final results	85
7.5	Analysis of results	95

8. Conclusion and future work	98
Appendices	102
Bibliography	104

List of Figures

2.1	The states of polarization of light	9
2.2	Light source with polarized and unpolarized components	11
2.3	Double diffraction in birefringent crystal	14
2.4	Step index Single-Mode Fiber	14
2.5	Some Hi-Bi fiber structures	17
2.6	Converging Lenses	18
2.7	Microscope objective	19
2.8	Quarter-wave retarder plate	20
2.9	Glan-Thompson polarizer	21
2.10	Wollaston prism	22
3.1	An electric circuit	28
3.2	A magnetic circuit	28
3.3	Geometrical shapes of cores	33
3.4	Core with air-gap	34
3.5	A typical hysteresis loop	34
4.1	Concept of Faraday effect	36
5.1	The principal components of the technique	40
5.2	The relationship between the output signal 'S' and the fiber length ℓ_1	47
5.3	Initial experimental set-up	48
6.1	Cleaved fiber facet	52
6.2	Magnetic head with air gap	55

6.3	Magnetic head with moving assembly	57
6.4	Schematic representation of dual path measuring method	59
6.5	Schematic diagram for dual path detection	61
6.6	The photo-detection and signal processing circuit	62
6.7	The experimental measurement system	64
7.1	Initial experimental set-up	69
7.2	Fiber F-SPV @ 632nm under no magnetic field	70
7.3	Fiber F-SPV @ 632 nm under no magnetic field	70
7.4	Beat lengths measured in F-SPV @ 632nm using (DC) magnetic field	71
7.5	Beat lengths measured in F-SPV @ 632nm using (DC) magnetic field	72
7.6	Beat lengths measured in F-SPV @ 632nm using (AC) magnetic field	73
7.7	Beat lengths measured in F-SPV @ 632nm using (AC) magnetic field	74
7.8	Beat lengths measured in F-SPZ @ 814nm using (DC) magnetic field	74
7.9	Beat lengths measured in F-SPZ @ 814nm using (DC) magnetic field	75
7.10	Faraday rotation vs light wave length	75
7.11	The final experimental set-up	79

7.12	Beat lengths measured in F-SPV @ 632nm using (DC) magnetic field with improved set-up	80
7.13	Beat lengths measured in F-SPV @ 632nm using (DC) magnetic field with improved set-up	80
7.14	Beat lengths measured in F-SPA @ 632nm using (DC) magnetic field with improved set-up	81
7.15	Beat lengths measured in F-SPA @ 632nm using (DC) magnetic field with improved set-up	81
7.16	Beat lengths measured in F-SPM @ 814nm using (DC) magnetic field with improved set-up	82
7.17	Beat lengths measured in F-SPM @ 814nm using (DC) magnetic field with improved set-up	83
7.18	Beat lengths measured in F-SPZ @ 814nm using (DC) magnetic field with improved set-up	84
7.19	Beat lengths measured in F-SPV @ 632nm using (DC) magnetic field - final results	84
7.20	Photograph of final experimental set-up	85
7.21	Beat lengths measured in F-SPV @ 632nm using (DC) magnetic field - final results	87
7.22	Beat lengths measured in F-SPV @ 632nm using (DC) magnetic field - final results	87
7.23	Beat lengths measured in F-SPA @ 632nm using (DC) magnetic field - final results	88
7.24	Beat lengths measured in F-SPA @ 632nm using (DC) magnetic field -final results	89

7.25	Beat lengths measured in F-SPM @ 814nm using	
	(DC) magnetic field - final results	89
7.26	Beat lengths measured in F-SPM @ 814nm using	
	(DC) magnetic field - final results	90
7.27	Beat lengths measured in F-SPZ @ 814nm using	
	(DC) magnetic field - final results	90
7.28	Beat lengths measured in F-SPZ @ 814nm using	
	(DC) magnetic field - final results	91
7.29	Beat lengths measured in F-SPV @ 814nm using	
	(DC) magnetic field	93
7.30	Beat lengths measured in F-SPV @ 814nm using	
	(DC) magnetic field	93
7.31	Beat lengths measured in F-SPA @ 814nm using	
	(DC) magnetic field	94
7.32	Beat lengths measured in F-SPA @ 814nm using	
	(DC) magnetic field	94

List of Tables

3.1	A comparison between electric and magnetic circuit	29
6.1	Noise factor improvement results	63
7.1	Data of fibers used in experiment	67
7.2	Beat lengths measured for various fibers	95

List of symbols and abbreviations

A	Toroid cross-sectional area
B_F	Birefringence
B	Magnetic flux density
c	Velocity of light in a vacuum
E	Electric field intensity
FOCS	Fiber optics communication systems
F	magneto-motive force (mmf)
H	Magnetic field density
Hi-Bi	High birefringence
I	light intensity detected by photodiode
J	Current density
Lo-Bi	Low birefringence
L	Mean length of turn
ℓ	Length of a segment of fiber
ℓ_b	Beat length
l_a	Air gap length
l_i	Length of the core
N	Number of turns of coil
n	refractive index of the medium
n_+	refractive index of the right circularly polarized component of the light
n_-	refractive index of the left circularly polarized component of the light

PM	Polarization maintaining fiber
S	Output signal
SOP	State of polarization
V	Verdet constant
ω	angular frequency
\mathcal{F}	Applied ampere-turn
ρ	Conductivity
\mathcal{E}	Electric potential gradient
Ω	Faraday rotation angle
ω_L	Larmor frequency
ϕ	Magnetic flux
\mathfrak{R}	Magnetic reluctance
μ	permeability of the medium
μ_0	permeability of vacuum
α	Phase shift caused by the birefringence
χ	susceptibility of the medium
λ	Wavelength

Chapter 1

1.1 Introduction

In today's society the need to transmit vast amounts of data has encouraged scientists and engineers to utilize the various properties of light to build efficient, low cost and very high speed fiber optics communication systems (FOCS). The use of polarized light is one way of providing very large bandwidth FOCS.

Recently, attention has been directed to applications that depend upon the state of polarization (SOP) of the light. Nominally, circular core fibers do not maintain the input SOP of light for more than a few meters, thus new fibers have had to be specially designed to meet this need. These single mode fibers are able to maintain a SOP over large distances.

The polarization maintaining (PM) capability of these fibers can best be described in terms of its modal birefringence. This wavelength independent parameter is a function of the difference in the effective refractive indices between the two orthogonally polarized modes, which together make up the single mode signal, and it is related to the beat length [1]:

$$\text{Birefringence } (B_F) = \lambda / \ell_b \quad (1.1)$$

where λ is the free space wave length and ℓ_b is the beat length of the fiber. Modal birefringence is convenient for comparing PM fibers fabricated for different wavelengths of light since beat length is dependent on the wavelength. The beat length is also the length of fiber required for the two orthogonally polarized modes to slip in phase by 360° .

According to their modal birefringence strength PM fibers are normally classified into two categories: low-birefringent (Lo-Bi) fibers and high-birefringent (Hi-Bi) fibers. Since the birefringence (Eq.1.1) of PM fibers is inversely proportional to beat length Hi-Bi fibers have small beat lengths, typically a few millimetres. Beat length is a key parameter when determining the application of a particular fiber and in optical fiber Gyroscopes it is used to predict system performance. Various techniques to measure beat length have already been developed but there is still room for improvement since all existing techniques have various limitations such as: the destruction of the fiber, necessary removal of the fiber jacket, inability to measure long lengths of fibers, inaccuracy, complicated methodologies, physical limitations and cost [2]. A novel technique proposed by Zhang [2] to measure small beat lengths in Hi-Bi fibers requires more research and development and this is the main objective of the current work.

1.2 Literature Review

PM fibers are used in many areas such as coherent optical communications, integrated-optic devices, and fiber sensors. For these applications it is often important to know the modal birefringence or the beat length of a fiber since the system performance is dependent upon it [3].

Various techniques to measure the beat length have already been developed. The cutback method is used for measuring the SOP by cutting pieces off the fiber end [4]. This method is destructive and relatively inaccurate, though it is applicable to any wavelength [1,4]. A twisting method used for stabilizing polarization states by rotating the fiber is useful for measuring a long beat length together with characterizing the twisting effect. Samples of optical fibers with a beat length down to 3.9mm have been measured successfully [5], however large errors arise if initial twisting is not taken into account [1,5].

The Scattering method [6] is used because of its simplicity and the characteristic fiber length (beat length) is obtained from the scattered light intensity. This method has a number of shortcomings such as : a) a high intensity power laser is needed due to the weakness of the observed scattered signal light and b) this method can not be applied at wavelengths above 700nm as they are invisible to the human eye. Various other methods have been reported for measuring

beat length such as the wave length sweeping technique, polarization optical time-domain reflectometry (POTDR) and the photo-elastic modulator method [5].

All the methods described above are traditionally used to measure beat length in Lo-Bi fibers [1] and to date only a few techniques have been proposed to measure the beat length of Hi-Bi fibers. Since the beat length in Hi-Bi fibers is very small, typically a few millimetres, high measurement resolution is needed. One technique proposed is the wavelength scanning technique [3]. This method is used to measure modal birefringence in fibers with polarization beat lengths in the range 0.5mm - 50mm. It combines an interferometric technique with wavelength scanning and permits a precise non-destructive measurement of the birefringence along different sections of a long optical fiber. The authors claim an accuracy of approximately 0.1% in the spectral range of 600nm - 850 nm [3]. However, this technique is costly and has a relatively complicated operation.

Over the past few years there have been a number of implementations, based on the Faraday magneto-optic effect, to measure the birefringence and Verdet constant [7]. The proposed technique uses the Faraday effect to measure small beat lengths in Hi-Bi fibers. This technique is simple, efficient and in principle beat lengths of less than 0.5 mm can be measured - which fulfills the beat length measurement requirements for currently available PM fibers [2].

1.3 Thesis outline

The aim of this thesis is to investigate the feasibility of the proposed beat length measurement technique. The thesis outline is as follows:

- A broad background on optics and magnetism is given in chapters 2 and 3 respectively.
- The basic principle of the Faraday magneto-optic effect is covered in chapter 4.
- The principles and implementation details of the proposed technique are discussed in chapter 5.
- In chapter 6, the practical aspects of the physical design of the proposed beat length measurement instrument is given, including problems faced and their solutions.
- The experimental procedures, results, and analysis are presented in chapter 7.
- Chapter 8, concludes with the improvement obtained using the proposed technique and discusses the scope for future work.

Chapter 2

Optics

2.1 Light

Light cannot be thought of as either a system of waves alone or a system of particles alone. Sometimes it acts as waves and sometimes as particles, but neither explanation can be considered complete in itself. When light interacts with matter it exhibits wavelike or particle-like properties depending upon the nature of the reaction. Philosophers and scientists have held six major theories concerning the nature of light over the last 3000 years. These are known as tactile theory, the emission theory, the corpuscular theory, the wave theory, the electromagnetic theory, and the quantum theory [8]. The last two theories of light combined, provides a more complete description of light, called quantum electro-magnetic theory. It is a comprehensive theory which includes both wave and particle properties of light. The phenomena of light propagation may be best described by the electro-magnetic wave theory, while the interaction of light with matter, in the processes of emission and absorption can be considered a quantum phenomena. Both phenomena are used in this research, that is, the propagation of light through the fiber and other optical components and the emission and absorption of the

light by the laser and photodiode respectively.

Light is, by definition, the visible portion of the electro-magnetic spectrum, covering the wavelength range between 400nm and 700nm. The wavelengths used in FOCS are not precisely defined but it is held to extend from the ultraviolet region (approx. 300nm) through the visible region and into the mid-infrared region (approx. 3000nm) of the electro-magnetic spectrum.

The transverse vibrations or oscillations of light waves makes them behave very differently from the more common sound wave which is longitudinal in nature. Some of the properties of light are its ability to be reflected, diffused, refracted, dispersed, diffracted, absorbed and scattered. These properties are significant in generating, propagating and detecting the light energy.

2.2 Polarized light

The polarization of light was first discovered by a Danish professor Erasmus Bartolinus and described in a publication in 1669 [9]. This reference concerned the refraction seen in a crystal called Iceland Spar, now called Calcite, and which is composed of calcium carbonate. After extensive work on this phenomena by Huygens, Malus, Brewster and Young, the theory of polarization is now generally considered well developed.

Polarized light is light whose electric field is

made to vibrate in one specific direction by means of passing it through some medium. This means that polarized light is a "labelled" light. The label on ordinary light is installed by the medium such as glass or crystal through which the light is passed. The label on the polarized light tells about the type of polarized light, that is linear, circular, elliptical and also the angle of the polarized light. Ordinary light is either unpolarized such as with an incandescent lamp light or partially polarized such as with sunlight. For example when light passes through a polarizer or retarder the future orientation of the incident light such as the SOP is determined, that is the polarizer or retarder labels some specific information on the light.

Theoretically a polarized beam of light is one in which the electric fields of all the waves are in the same direction. The beam is said to be linearly polarized if a single electric-field vector perpendicular to the direction of propagation can represent the beam, see Fig.2.1a [9]. If the electric fields are in random directions, the beam is unpolarized. Any vector representing a linearly polarized beam or wave can be resolved into a pair of mutually perpendicular or orthogonal components (x and y) of the electric field, travelling along the direction of propagation.

If the two components along the x and y axes are equal in amplitude, but are 90° out of phase, then the resultant wave is said to be circularly polarized. This state

is shown in Fig.2.1b. Circularly polarized states are distinguished by the sense of rotation of the vector. The state shown in Fig.2.1b represents a right circular polarization as the resultant total polarized vector rotates clockwise when viewed towards the source. Linearly polarized light is specified by its amplitude. Circular polarized light is specified by its amplitude and the sense of rotation (left or right) [9].

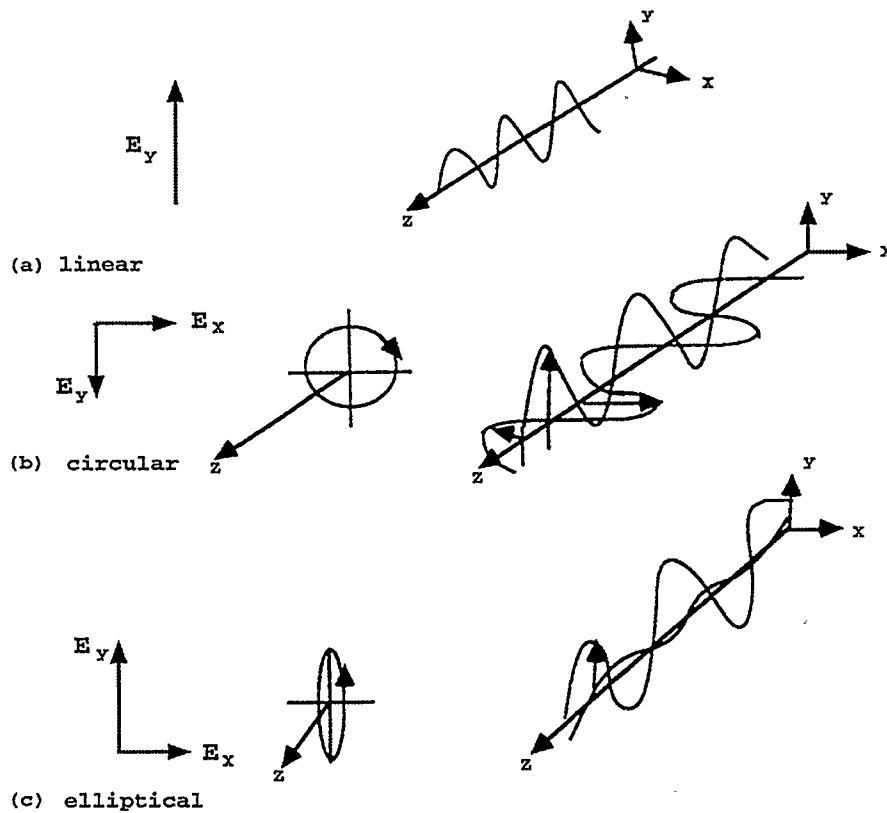


Fig.2.1 The states of Polarization of lightwave.

If x and y components of unequal amplitude are added the result is elliptically polarized light as shown in Fig.2.1c. This wave is now characterized by its amplitude and ellipticity and by the orientation of the major axis of the ellipse with respect to a reference axis. It is often convenient to consider elliptically polarized light as the sum of a circular and a linear component [9].

Various materials effect light differently in that they induce a different direction of polarization and these substances can be used to prepare devices that permit only light polarized in a certain direction to pass through them.

2.3 Mathematics of polarized light

Many scientists such as Stokes and Jones, [10] have already developed mathematics to represent polarized light and its interaction with optical systems. Definitions of polarized light are represented in Fig.2.2 [11].

In Fig.2.2, I_u represents the intensity of unpolarized and I_p represents the intensity of polarized light. The most general representation of the polarization state is by way of the Stokes parameters (S_0, S_1, S_2, S_3). The Stokes parameters do not give direction of propagation, wavelength or overall phase. They are related to the azimuth α and ellipticity Γ of the polarized component, the degree of polarization 'p' and the overall intensity 'I'.

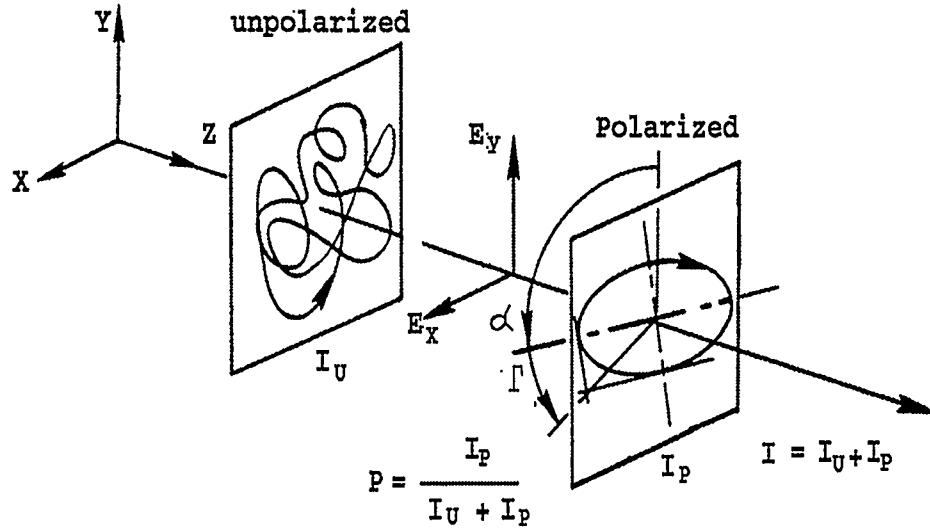


Fig.2.2 Light source with polarized and unpolarized components.

As shown in Fig.2.2, the azimuth α , $(-90^\circ, 90^\circ)$, is measured counter-clockwise from the x-axis to the ellipse major axis, looking towards the source. Ellipticity Γ , $(-45^\circ, 45^\circ)$ is the angle whose tangent is the ellipse axial ratio, taken positive for right handed polarization. The Stokes parameters are given below [11]:

$$S_0 = I \quad (2.1)$$

$$S_1 = S_0 p \cos 2\Gamma \cos 2\alpha \quad (2.2)$$

$$S_2 = S_0 p \cos 2\Gamma \sin 2\alpha \quad (2.3)$$

$$S_3 = S_0 p \sin 2\Gamma \quad (2.4)$$

Totally polarized light ($p=1$) has a constant phase and amplitude relationship between the orthogonal transverse field component, \mathbf{E}_x and \mathbf{E}_y . The two-element Jones vector $(\mathbf{E}_x, \mathbf{E}_y)$

completely describes such light, apart from its wavelength and direction of propagation. The complex polarization ratio ρ is defined and related to the other parameters as follows [15]:

$$\rho = E_x/E_y = \frac{1 - i \tan\Gamma \tan\alpha}{\tan\alpha + i \tan\Gamma} = \frac{S_2 - i S_3}{S_0 - S_1} \quad (2.5)$$

Light interaction with an optical system

An optical system interacts with totally polarized light in a manner described by a general (complex) linear transformation (2x2 Jones matrix) acting on the Jones vector.

$$\begin{bmatrix} E_{x0} \\ E_{y0} \end{bmatrix} = \begin{bmatrix} J_{xx} & J_{xy} \\ J_{yx} & J_{yy} \end{bmatrix} \begin{bmatrix} E_{xi} \\ E_{yi} \end{bmatrix} \quad (2.6)$$

The subscripts 'i' and 'o' refer to the input and output light respectively. The Jones matrix describes the change in overall phase since that information is contained in the Jones vector. To simplify the Jones matrix, one element may be factored out, J_{yy} for example, and still retain a complete description of the system's polarization-altering properties [11]. Only the overall intensity and phase change is lost and the resulting relationship among the normalized quantities is

$$\begin{bmatrix} \rho_o \\ 1 \end{bmatrix} = J_{yy} \frac{E_{yi}}{E_{yo}} \begin{bmatrix} a & b \\ c & 1 \end{bmatrix} \begin{bmatrix} \rho_i \\ 1 \end{bmatrix} \quad (2.7)$$

where ρ is the complex polarization ratio, given in (Eq.2.5)

and the subscripts 'i' and 'o' again refer to the input and output light respectively. The matrix equation (2.6) or (2.7) is equivalent to the bilinear transformation [11]

$$\rho_o = \frac{a\rho_i + b}{c\rho_i + 1} \quad (2.8)$$

In many cases of practical importance, the Jones matrix is diagonal, ($b=c=0$) and only the parameter "a" characterizes the interaction. It is then customary to write

$$a = J_{xx} / J_{yy} = \rho_o / \rho_i = \tan \psi \exp (i\Delta)$$

where ψ and Δ are the standard ellipsometric parameters.

In other cases, only the single parameter α or Γ is changed by the system. For example in materials exhibiting optical activity, the azimuth of the output light is rotated from that of the input light by an amount Θ . This interaction may be described by a Jones matrix with $a=1$, $c = -b = \tan\Theta$, but it is much simpler to write $\alpha_o = \alpha_i + \Theta$, where Θ is then the single system parameter of interest [11]. The Jones calculus is used to explain the interaction of polarized light with the designed system in chapter 5.

2.4 Birefringence

This effect is also known as double refraction [12]. Birefringence refer to the splitting of a single light beam into two beams inside a crystal such as quartz or calcite. The double refraction in the birefringent crystal calcite is shown

in Fig.2.3 [13].

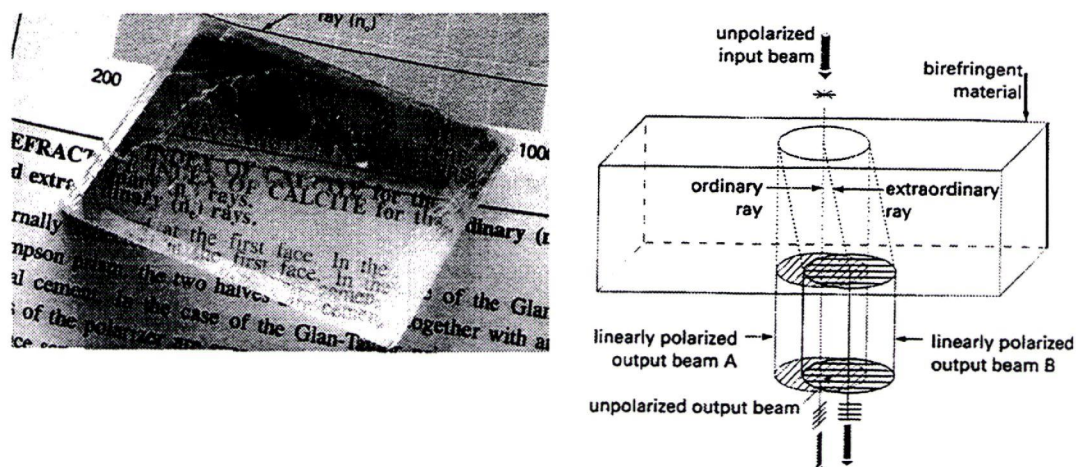


Fig.2.3 Double refraction in birefringent crystal.

If a light ray enters the crystal at an angle to the optic axis, then it is split into two rays. The polarization of one ray is perpendicular to the optic axis and it is called the ordinary (o) ray. The polarization of the other ray is orthogonal to the polarization of the o-ray and it is called the extraordinary (e) ray. The optic axis is the direction in the crystal for which there is no distinction between the o-ray and e-ray.

2.5 Polarization-Maintaining (PM) Fibers

It is known [14,15] that the state of polarization in ordinary single-mode fibers (SMF) can be altered due to external stresses such as bending, tension, kinks and twist. Rotation of the state of polarization due to external perturbations is attributed to changes in fiber birefringence causing noise,

drift and signal fading due to random coupling between the two propagating orthogonal modes (eigenmodes) within the fiber. This birefringence bias can be greatly reduced with the use of polarization maintaining (PM) fibers [15].

PM fibers are step index single-mode fibers (see Fig.2.4) in which stress applying elements inside the cladding induce anisotropy in the fiber core. Breakup of the cylindrical symmetry raises the polarization degeneracy of the fundamental spatial mode giving rise to two independent polarization modes. Because of the elasto-optic effect (a change in the refractive index of an optical fiber caused by variation in the length of fiber core in response to mechanical stress), the effective refractive index is significantly different for these two modes, which travel along the fiber with different group velocities. A number of different geometries have been conceived to induce the stress anisotropy and low loss PM fibers are now commercially available [16].

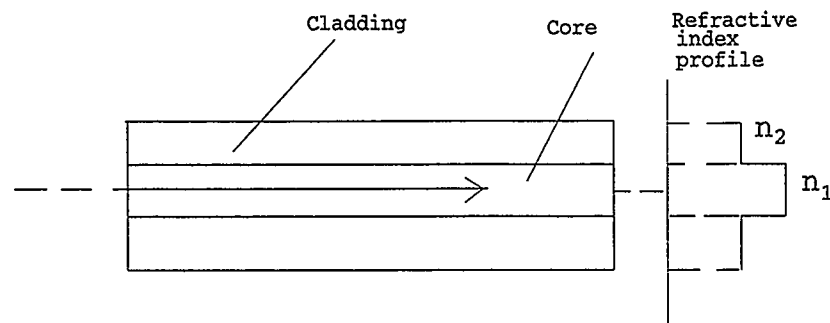


Fig.2.4 Step index single mode fiber.

The stress applying elements in the PM fibers are usually made of borosilicate glass whose thermal expansion coefficient is different from that of pure silica glass. The residual stress comes from the differential contraction of the silica and the stress applying elements when the fiber is drawn. Higher stress results in higher fiber birefringence [16].

2.6 Lo-Bi and Hi-Bi PM Fibers

PM fibers are mainly classified into two categories, low-birefringent (Lo-Bi) fibers and high-birefringent (Hi-Bi) fibers. In the Lo-Bi fibers, a linear-polarization wave and a circular-polarization wave can be propagated with small polarization dispersion. With present technology, however, SOP is sensitively dependent on external forces such as transverse pressure, bend and temperature. Conventional SMF, which belongs to this category, have been applied experimentally to long-span coherent optical-transmission systems. Hi-Bi fibers, where the SOP is very effectively maintained using present technology, are used in fiber optic gyroscopes, sensors and wave-length division multiplexing systems. Since the high birefringence of these fibers prevents coupling of power between the two orthogonal components these fibers are also very useful in communication as they have negligible noise and cross-talk. The measurement of birefringence or beat length in Hi-Bi fibers is required in order to incorporate it into

specific applications such as the optical fiber Gyroscope. The optical fiber gyroscope is rapidly replacing the conventional design in an ever increasing number of uses worldwide. The internal birefringence of Hi-Bi fibers is produced by the geometrical effect of the core and the stress effect around the core. The Hi-Bi PM fibers with the stress effect, so-called stress-induced birefringent fibers such as elliptical cladding fibers, elliptical jacket fibers, PANDA fibers and bow-tie fibers exhibit low optical losses and low cross-talk [1]. The geometrical shapes of some Hi-Bi PM fibers are shown in Fig.2.5.

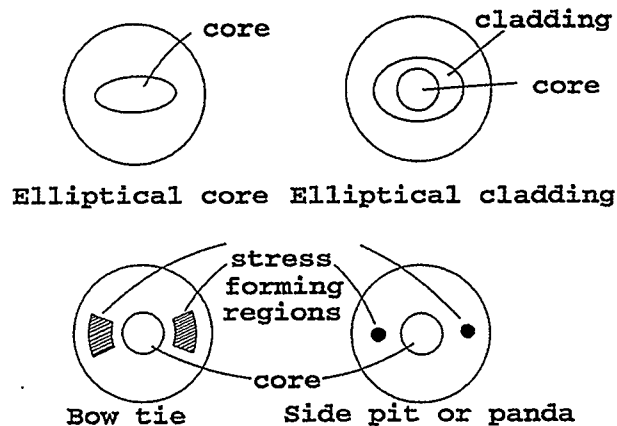


Fig.2.5 Some Hi-Bi fiber structures.

The PM fibers used in this research are Hi-Bi PM fibers from Newport Inc. and 3-M Inc.

2.7 Optical system components

Various optical components such as lenses and polarizers

are required to design an optical system. The selection, proper use and the position of these components are critical for optimum optical system performance. These optical components produce reflection, refraction, and other effects which together produce particular phenomena. The utilization or measurement of these phenomena are used to solve various practical problems.

2.7.1 Lenses

Lenses are used singly or in combination for beam reshaping and focusing. These lenses are usually made of optical glass or other transparent materials as free as possible from inhomogeneities. Double concave, plano-concave and concave meniscus are diverging lenses. Similarly, double convex, plano-convex and concavo-convex or convex meniscus are converging lenses which are thicker at the centre than at the edges, as shown in Fig. 2.6. [13].

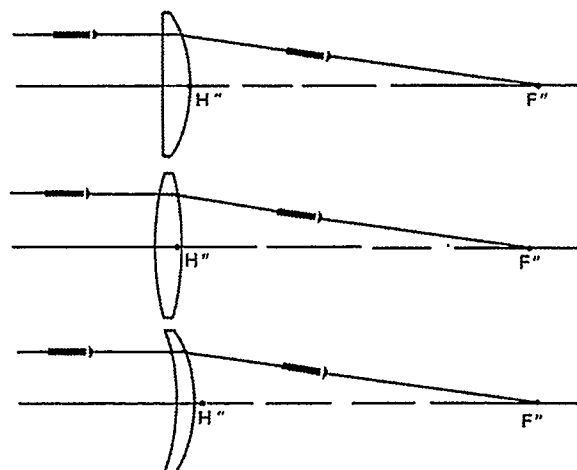


Fig.2.6 Some converging lenses.

In Fig. 2.6, F' is the focal point and H' is the secondary principal or nodal point. The Plano-convex lens (Melles-Griot # 01 LPX 198) with focal length 105 mm and concavo-convex lens (Oriel # 40209) with focal length 16 mm are used in this research. A microscope objective lens is made from a combination of basic lenses as shown in Fig. 2.7.

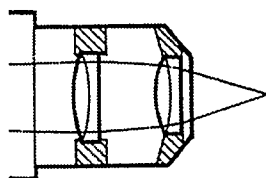


Fig.2.7 Microscope objective lens.

These objectives, available in different magnifying power, are designed to produce a desired magnification and optimize image quality when mounted in a standard housing [13]. A X10 microscope objective lens is used in this project. All three of the above lenses are used for beam focusing in this project.

2.7.2 Retarder

Linear retarders, sometimes called wave-plates, are optical components that introduce a specific phase shift between the orthogonal linearly polarized components of light transmitted through them. If the thickness of the plate is such that the phase difference (retardation of the slow ray by comparison with the fast ray at emergence) is $1/4$ -wavelength, the plate is called a quarter-wave plate. They are therefore

useful for modifying and controlling polarization states such as to convert linearly polarized light to circularly polarized light. These plates are made from birefringent materials, such as calcite. A quarter-wave retardation plate is shown in Fig. 2.8.

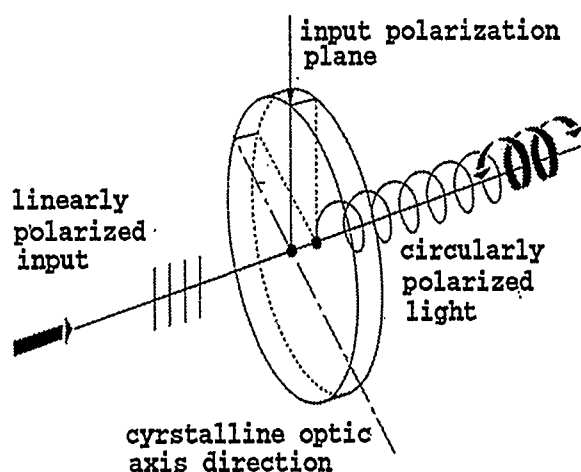


Fig.2.8 Quarter-wave retardation plate.

2.7.3 Polarizer (Glan-Thompson)

A polarizer creates linear polarization by transmitting only the desired plane of vibration or SOP and the unwanted orthogonal component is absorbed, or reflected or refracted at a different angle and out of the way [12]. A very common type of polarizer, the Glan-Thompson (Oriol# 25705), and used in this research is shown in Fig.2.9 [17].

The Glan-Thompson polarizer consists of two identical calcite prisms of triangular cross-section with their optic axes parallel to each other and to the input and output faces, separated by a layer of isotropic material such

as optical cement.

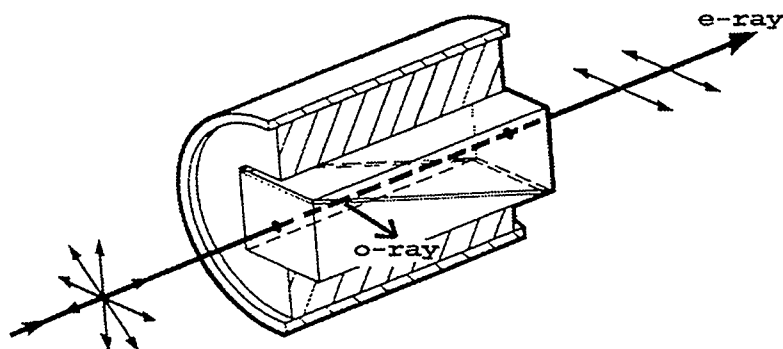


Fig.2.9 Glan-Thompson polarizer.

The main criterion for the polarizer is its extinction ratio which is the ratio of the optical power in the emitted orthogonal modes. A polarizer such as the Glan-Thompson can provide a very high extinction ratio in that it virtually eliminates the undesired orthogonal mode. The manufacturers specification for this polarizer gives an extinction ratio of 10^{-5} and an acceptance angle of 15 degrees at 515nm. The optical transmittance is high being 90% for the polarized ray from 350nm to 2500nm.

2.7.4 Prism (Wollaston)

The Wollaston prism, which splits the incoming light into two diverging orthogonally polarized output beams is a very significant component of this project. It consists of two prisms cemented together and made of birefringent, uniaxial material (usually quartz or calcite) [18]. As the light

travels through the first prism, both the ordinary and extraordinary beams travel co-linearly with different refractive indices. At the interface the beams are interchanged so the ordinary ray enters a medium of lower refractive index and is refracted away from the normal and the extraordinary beam enters a higher refractive index and is refracted towards the normal. This divergence angle between the two beams is increased further at the polarizer exit [17], as shown in Fig.2.10.

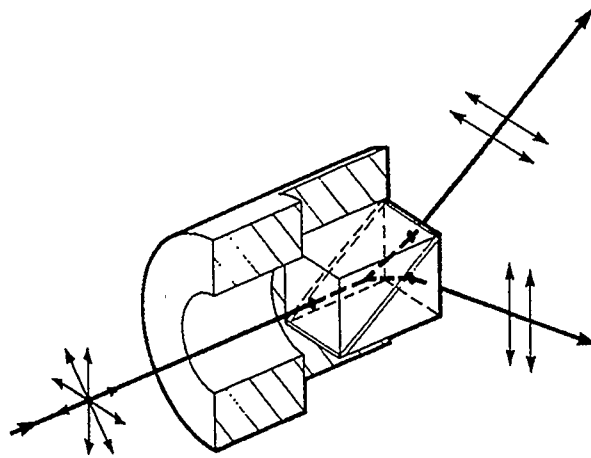


Fig.2.10 Wollaston prism.

The Wollaston prism (Oriel # 25695) used in this project has an angular separation between the two output beams which varies from 24° to 18° over the 350nm to 2500nm usable wavelength range.

2.7.5 Electro-optical components

The electro-optical components such as lasers and

photodiodes are the active components in a fiber optics system. In the case of the laser its fundamental function is to convert electrical energy into optical energy in an efficient manner and vice versa in the case of the photodiode.

a) Lasers

Lasers are the optical source. The most common types of lasers are made with gases such as Helium-Neon (He-Ne) and semiconductor materials such as Gallium Arsenide (GaAs). Gas lasers typically have higher output power than semiconductor lasers but have less output power stability. A He-Ne laser (Hughes) of wavelength 632.8nm with output power of 4mW and a Gallium Arsenide laser (GALA) of wavelength 814nm with output power of 1mW are used in this project.

b) Photo-diodes

The photodiode detector is also a key element in fiber optic systems since its function is to convert the received optical signal into an electrical signal which is then amplified for further processing. A matched pair of photodiodes (ECG # UV 100), also called Bi-cell, are used in this project for signal detection. The Bi-cell has low noise, low cross talk and good responsivity (0.62A/W at 900nm) in the 630nm to 900nm wavelength range. The matched pair of photodiodes greatly reduces the chances of introducing electronic errors into the detected signals.

2.7.6 Mechanical components

Mechanical precision plays an extremely critical role in polarimetry which requires, in many cases, the alignment of the optical components with sub-micron precision. There is a need not only to achieve this positional precision but also to maintain it once it has been achieved. A good example is a single-mode Hi-Bi fiber which typically has a core diameter of $2\mu\text{m}$ to $10\mu\text{m}$. To align this fiber core with a focused laser beam and to maintain good power transfer, an alignment precision of $< 1\mu\text{m}$ is required. Good mechanical precision provides repeatability of observations and accurate results. The steel translation stages used in this project provided smooth, controlled and reasonably repeatable linear motion for fiber and optical components. An X-Y-Z translation stage, with lens, is used to inject the collimated laser beam into the fiber and an X-Y translation stage is used at the output. Component holders with magnetic bases are used to hold laser, lenses, translation stages etc; and they provide a very stable system. Positioning rods of lengths from 8cm to 12cm are used in this project.

a) Vibration-isolated table

Vibrations, both natural and human based, are always part of any system and they produce relative motions of objects and surfaces. While these are often imperceptible to the casual observer they may be disastrous to a wide range of

precision experiments such as polarization measurement. Typical laboratory environments are continuously subjected to ambient vertical vibrations in the range of 10Hz to 30Hz. Vibrations due to equipment and machinery often have a somewhat higher frequency but are usually below 200Hz [13]. Precision optical systems depend upon reliable positional stability. Virtually all unwanted motions must be removed from the entire system since failure to do so may result in component misalignment and possible data errors.

The optical tabletop and its associated vibration-isolating support system are specifically designed to provide the stable and physically invariant environment required for experimentation and development. This is because an optical table is designed to have minimal response to a deflective force or vibrations. These systems are designed to prevent (or quickly dampen out) relative motion between components mounted on a tabletop surface, whether these motions are as a result of a bending and twisting deflection of the entire table structure, external vibrations or shocks being coupled into the table structure, or even a vibration source mounted on the tabletop surface [13].

A vibration-isolated table Micor-g, model # 63-531, manufactured by Technical Manufacturing Corp; U.S.A was used to obtain the final results of this research.

Chapter 3

Magnetics

3.1 Magnetism

3.1.1 History

The first recorded magnetic phenomena observed were those associated with naturally occurring magnets that is, magnetized fragments of iron ore found near the ancient city of Magnesia (whence the term "magnet"). These natural magnets attract un-magnetized iron and the effect is most pronounced at certain regions of the magnet known as its poles. This effect was known to the Chinese as early as 121 A.D. and the use of magnets as aids to navigation can be traced back at least to the Eleventh century [19].

The study of magnetic phenomena was confined for many years to natural magnets and not until 1819 was any connection between electrical and magnetic phenomena shown. Oersted demonstrated that the magnetic effect could be produced by moving electric charges and Faraday and Henry showed that current could be produced by moving magnets close to wires [19]. Faraday also demonstrated the effects of a magnetic field on light. The enormous research contributions of many other scientists such as Ampere, Lenz, Maxwell and

Hertz are also appreciable in the development of the laws and theories of magnetism.

3.1.2 Electro-magnetics

Besides natural magnets, it is possible to produce magnetic fields with electricity using ferromagnetic materials such as iron, this type of magnet being known as the electro-magnet. A coil of N turns carrying current I around a ferromagnetic core produces a magnetomotive force (mmf) given by NI . The symbol F is sometimes used for this mmf and the units are ampere-turns. Amperes's law provides the basic relationship between the F and NI as

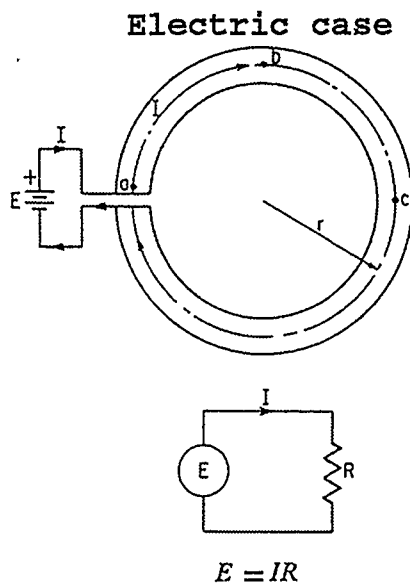
$$F = NI = \oint \mathbf{H} \cdot d\mathbf{l} = \mathbf{H}L \quad (\text{under certain conditions})$$

where H is the magnetic field intensity and L is the path length. Thus $\mathbf{H} = N \mathbf{I} / L$ (3.1)

The unit for H in the MKS system is Ampere-turn/meter, and in the CGS system it is the Oersted. Another quantity which is related to electro-magnetics is the magnetic flux density B , also known as the magnetic induction intensity. It is the flux per unit area normal to the direction of the magnetic path and the H and B are related by the relationship $B = \mu H$, where μ is the permeability and it is a fundamental property of the medium. The units for B in the MKS system is the Tesla, and in the CGS system is lines/cm² or Gauss.

A comparison [20] between electric and magnetic

circuits is given in Table 3.1. For the electric case the toroidal copper ring is assumed open by an infinitesimal amount with the ends connected to a battery. A current of I amperes flows through the ring as shown in Fig.3.1. For magnetic case the toroidal iron ring is assumed wound with N turns of wire with a current i flowing through it and the magnetomotive force creates the flux ϕ , as shown in Fig.3.2 [25]. Their equivalent circuits are also given.



**Equivalent
Circuits**

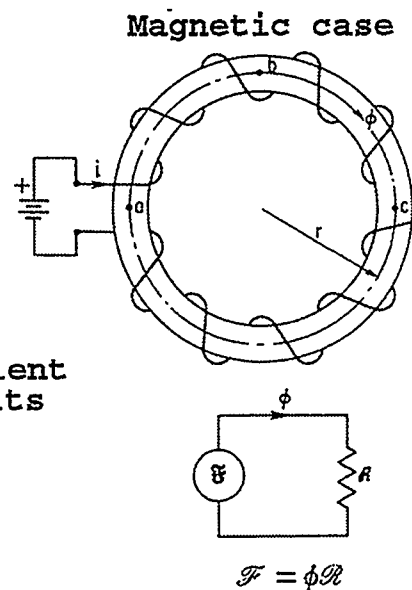


Fig.3.1

Fig.3.2

Comparison of Electric and Magnetic circuits.

Table 3.1

ELECTRIC CASE	MAGNETIC CASE
<p>Driving Force</p>	<p>Driving Force</p>
<p>applied battery voltage = E</p>	<p>applied ampere-turns = \mathcal{F}</p>
<p>Response</p>	<p>Response</p>
<p><u>Driving force</u></p>	<p><u>Driving force</u></p>
<p>current = electric resistance</p>	<p>flux = magnetic reluctance</p>
<p>$I = E / R$</p>	<p>$\phi = \mathcal{F} / \mathfrak{R}$</p>
<p>Impedance</p>	<p>Reluctance</p>
<p>Impedance is a general term used to indicate the impediment to a driving force in establishing a response.</p>	<p>Reluctance = $\mathfrak{R} = L / \mu A$ where $L = 2 \pi r$ = mean length of a turn of the toroid and A is the toroidal cross-sectional area (same in electric case)</p>
<p>Resistance = $R = \rho L / A$</p>	
<p>Current Density</p>	<p>Flux Density</p>
<p>By definition, current density is current per unit area, thus</p>	<p>Flux density is expressed as Webers per unit area. Thus</p>
<p>$J = I / A$ $= \mathcal{E} / \rho$</p>	<p>$B = \phi / A$ $= \mu H$</p>

Continued on next page

ELECTRIC CASE	MAGNETIC CASE
<p>Electric field intensity</p> <p>With the application of the voltage E to the homogeneous copper toroid, there is produced within the material an electric potential gradient given by</p> $\mathcal{E} \equiv E / L = E / 2 \pi r$ <p>in V/meter</p> <p>The closed line integral of \mathcal{E} is equal to the battery voltage E.</p> <p>Thus $\oint \mathcal{E} dl = E$</p>	<p>Magnetic field intensity</p> <p>When a magnetomotive force (mmf) is applied to the homogeneous iron toroid, there is produced within the material a magnetic potential gradient given by</p> $H \equiv \mathcal{F} / L = \mathcal{F} / 2 \pi r$ <p>in AT/meter</p> <p>By Ampere's circuital law, the closed line integral of H equals the enclosed mmf force. Thus $\oint H dl = \mathcal{F}$</p>
<p>voltage drop</p> <p>If it is desired to find the voltage drop occurring between the two points a and b of the copper toroid, it will be $V_{ab} = I R_{ab}$ where R_{ab} is the resistance of the copper toroid between points a and b.</p>	<p>mmf drop</p> <p>The portion of the total applied mmf appearing between points a and b is found similarly:</p> $\mathcal{F}_{ab} = \phi \mathcal{R}_{ab}$ <p>where \mathcal{R}_{ab} is the reluctance of the iron toroid between points a and b.</p>

It should not be inferred from the foregoing that the electric and magnetic circuits are analogous in every respect [20]. For example there are no magnetic insulators analogous to those known to exist for electric circuits. Also when the direct current is established and maintained in an electric circuit, energy must be continuously supplied. An analogous situation does not prevail in the permanent magnet case where a flux can be established and maintained constant without any external energy being supplied [20].

3.2 Magnetic cores

3.2.1 Magnetic materials

These materials are made of iron or alloys (often iron mixed with various metals such as nickel or aluminum) to obtain the required magnetic flux with low applied electrical energy and low losses. According to their chemical compositions, production methods and applications, they are classified into two main types: 1) hard magnetic materials and, 2) soft magnetic materials. The hard magnetic materials such as Alinco 5 have a wide hysteresis loop i.e. maximum coercive force to obtain a stable and strong magnetic field and they are used in electrical instruments, loudspeakers, telephones, etc. The soft magnetic materials should have a high permeability (for low losses) and a very narrow hysteresis loop with a negligible coercive force. These materials are subdivided into various groups such as pure

iron, sheet electro technical Silicon iron, high permeability alloy (Permalloy)). The high permeability alloys such as Fe-Ni-Co have low magnetic losses and are good to design electromagnets with but they are costly. For this project a soft steel core was used. A table of hard and soft magnetic materials is given [24] in the appendices.

3.2.2 Magnetic cores

Magnetic cores the configurations of magnetic materials that are placed in a rigid spatial relationship to current carrying conductors and whose magnetic properties are essential to its use. For example, it may be used: (1) to concentrate an induced magnetic field as in a transformer, induction coil, or armature: (2) to retain a magnetic polarization for the purpose of storing data: or, (3) for its non-linear properties in a logic element. The geometrical shapes of various cores are given in Fig.3.3.

Magnetic cores are made of various magnetic materials such as iron and its alloys. In this project, a square soft steel core is used to make the magnetic head.

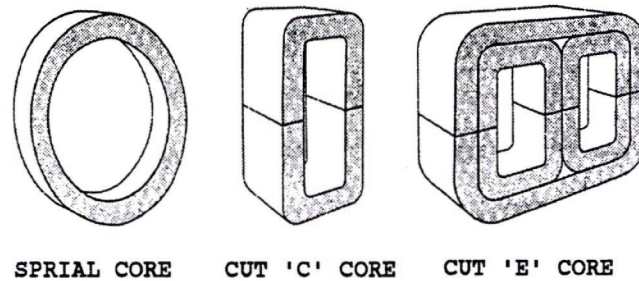


Fig.3.3 Geometrical shapes of magnetic cores.

a) Magnetic Cores with air gaps

Magnetic circuits with small air gaps are very common [21]. The gaps are generally kept as small as possible since the NI drop of the air gap is often much greater than the drop in the core. The flux fringes outward at the gap so that the equivalent area at the gap exceeds the area of the adjacent core. Provided that the gap length l_a is less than $1/10$ the smaller dimension of the core (a or b) an apparent area, S_a , of the air gap can be calculated. For a rectangular core with cross-sectional dimensions a and b then [21]

$$S_a = (a + l_a) \times (b + l_a)$$

Referring to Fig.3.4, for a uniform iron core of length l_i with a single air gap, Ampere's law reads

$$NI = H_i l_i + H_a l_a = H_i l_i + (l_a \phi / \mu_0 S_a) \quad (3.2)$$

Fig.3.4 shows a core with an air-gap similar to the one used in this project. A detailed calculation for the magnetic head is given in Chapter 6.

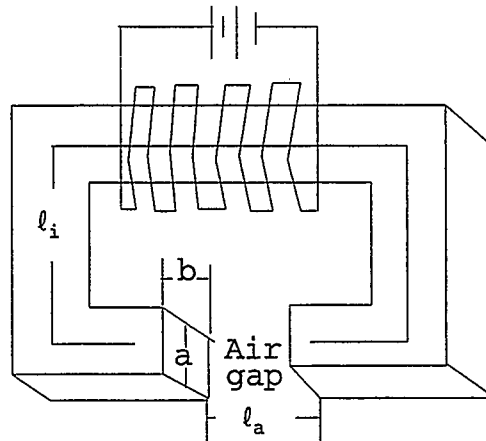


Fig.3.4 Core with air gap.

b) Magnetic Core losses

There are two types of core losses: Hysteresis loss and Eddy current loss.

1) Hysteresis loss: A hysteresis loop is shown in Fig.3.5 [20]:

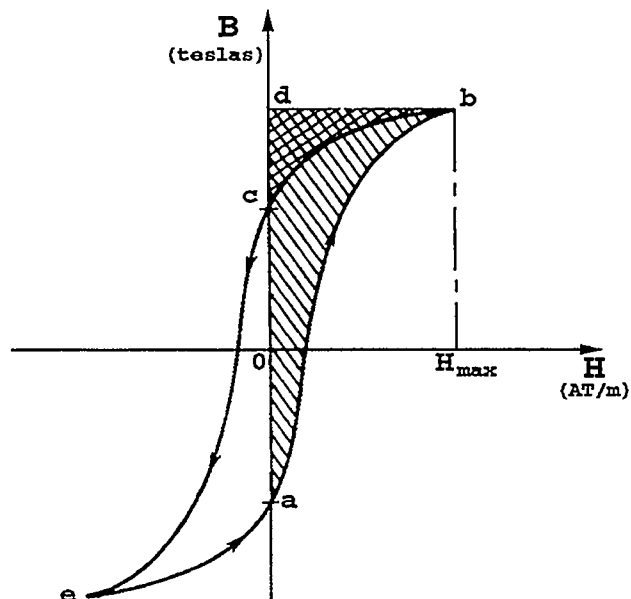


Fig.3.5 Typical hysteresis loop.

This loop shows the variation of the flux density B as a function of magnetic field intensity H for a ferro-material in a cyclic condition. In the figure, area $abdca$ represents the energy stored in a core and the area $bdcba$ represents the energy release by the core. The difference between these areas represents the amount of energy which did not return to the source but rather is dissipated as heat and this energy loss is the hysteresis loss of the core.

2) Eddy current loss Another loss is subjected to the time varying fluxes - the eddy current loss [20]. This is the power loss associated with the circulating current that is found to exist in a closed path within the body of a ferro material causing an undesirable heat loss. The circulating current is created by the differences in potential existing throughout the body of material owing to the action of changing flux. The core losses effect temperature rise and the rating of the electromagnetic device.

Chapter 4

Faraday Magneto-optic effect

The interaction of light with matter is related to the electronic structure of the matter. In particular this interaction is affected by the magnetic state of the medium and it gives rise to the magneto-optic effect. The existence of this effect is a strong affirmation of the electromagnetic nature of light [22]. In 1845, Michael Faraday discovered that when a block of glass is subjected to a strong magnetic field, it becomes optically active [23]. The Faraday magneto-optic effect is shown in Fig.4.1 [24].

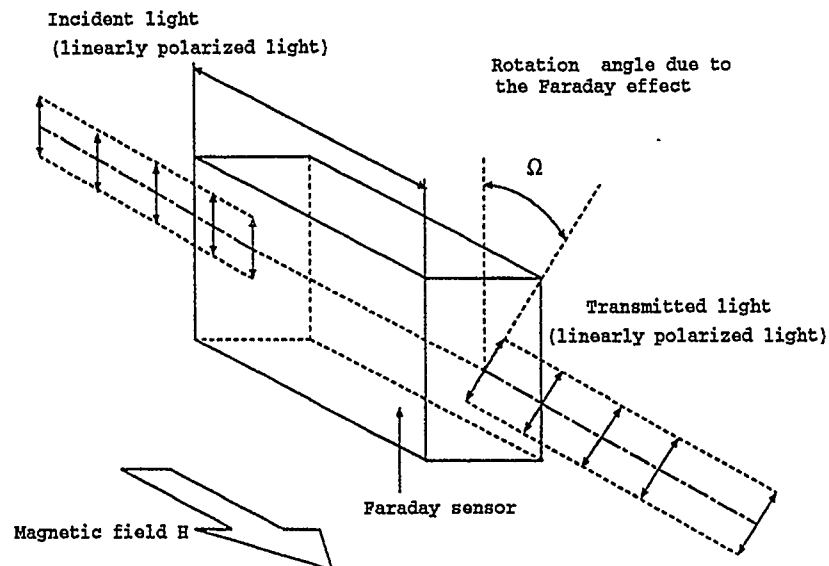


Fig.4.1 Concept of Faraday effect.

In Fig.4.1 when the linearly polarized light propagates through the glass in a direction parallel to the applied magnetic field the SOP of the light is rotated. This rotation is referred to as the Faraday rotation and the degree of rotation is proportional to the magnetic field strength H and the distance the light travelled through the medium. This rotation can be expressed by

$$\Omega = V H L \quad (4.1)$$

where

Ω is the angle of rotation, also called Faraday rotation,

V is the Verdet constant,

H is the magnetic field intensity component in the direction of light propagation, and

L is the path length of the Faraday sensor such as the block of glass. The above relationship was first suggested by Wiedemann (1851) and later by Verdet (1854) [24]. In the past few years, there have been a number of implementations of the Faraday magneto-optic effect in an attempt to measure the birefringence and Verdet constant [24]. In this research, the Faraday magneto-optic effect is used to measure the beat length in Hi-Bi fibers.

The Verdet constant is generally described by microscopic theory and it is temperature and wavelength dependent [24]. The effect of magnetic fields upon right and left circularly polarized components is different, namely refractive indices

and propagation constants are different for each sense of polarization, and a rotation of the state of polarization of linearly polarized waves is observed. If there is absorption in the medium then the absorption coefficient will also be different for each sense of circular polarization and the emerging beam will then be elliptically polarized.

In 1825 Fresnel showed that for natural optical rotation the plane-polarized wave could be considered as right and left circularly polarized waves travelling through the medium at different velocities. The rotation of the plane of polarization for light passing through a material of length L is given by [10]

$$\Omega = (\omega L/2c) (n_- - n_+) \quad (4.2)$$

where ω is the angular frequency, n_+ and n_- are the refractive indices of the right and left components, and c is the speed of light. Since this description does not depend on the manner in which the differing velocities arise it is also applicable to magnetic induced rotation.

Rotation arises through the coupling of electro-magnetic radiation with the electrons or bound oscillators. The magnetic field can be taken into account by using a moving coordinate system which relates to Larmor frequency $\omega_L = eH/2mc$, where e and m are, respectively, the magnitude of the charge and the mass of the electron. The two components

of the radiation then have the angular frequencies $\omega - \omega_L$ and $\omega + \omega_L$. From the equation for the rotation given above, Ω is then given by

$$\begin{aligned}\Omega &= [n(\omega - \omega_L) - n(\omega + \omega_L)]\omega L/2c \\ &= (\omega L\omega_L/c) (dn/d\omega)\end{aligned}\tag{4.3}$$

where n is refractive index of the medium and eq.4.3 is called the Becquerel equation [24].

All dielectric materials exhibit this Faraday effect, or induced birefringence, to some extent. In particular it is found that glasses and silica, the materials from which optical fibers are constructed, have readily measurable Verdet constants, so optical fibers also exhibit the Faraday effect [7]. As silica has a relatively small Verdet constant it is necessary to have a strong magnetic field in order to measure the Faraday effect in optical fibers.

Chapter 5

Beat length measurement technique

5.1 Basic Principle

It has already been stated in a previous section that the proposed technique for beat length measurement in Hi-Bi fiber using the Faraday magneto-optic effect has significant advantages over various existing techniques such as high accuracy, simple construction and easy operation. The proposed technique involves magneto-optic modulation. The principle components used in this technique are shown in Fig. 5.1.

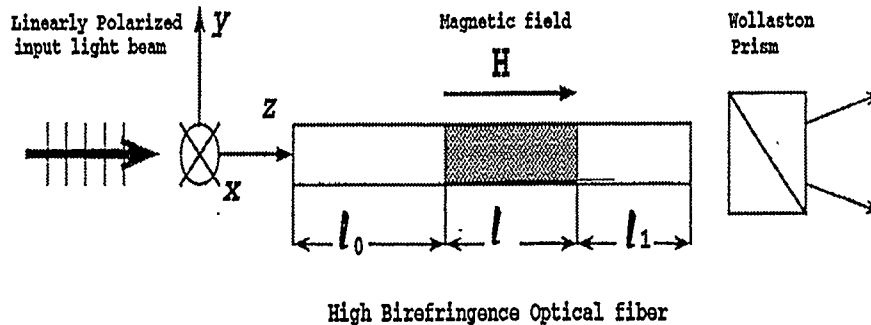


Fig.5.1 The principle components for the measurement of the beat length in Hi-Bi fiber.

A linearly polarized light beam is input into the Hi-Bi optical fiber and the intensities of the two Wollaston prism

output beams, I_1 and I_2 , are equalized using the rotating polarizer before applying the magnetic field. This is done in order to detect a change in the intensity of either beam after the magnetic field is applied. When a magnetic field is applied to a particular section of the fiber, then because of the Faraday effect, the linearly polarized beam will be rotated by some angle in this section of the fiber. The rotation at this section results from the anisotropy of the fiber material and it is due to applied strong magnetic field. The anisotropy of the fiber material changes the birefringence of the fiber which results in the rotation of the linearly polarized input beam. At the output end of the fiber the 'rotated' light beam is divided into two beams by the Wollaston prism. The rotation of the linearly polarized output beam varies the intensities of the two beams at the output of the Wollaston prism though the total intensity or power remains constant. These two beams are converted into electronic signals by two photo-detectors at the signal processing unit. The beat length of the fiber can then be determined by analyzing the changes in the electrical signals corresponding to the movement of the electro-magnet along the length of the Hi-Bi optical fiber [2].

5.2 Mathematics of the technique

As shown in Fig.5.1, the Hi-Bi fiber to be measured is divided into three segments (ℓ_0 , ℓ , ℓ_1), and the

corresponding phase differences caused by the birefringence in these segments are expressed by α_0 , α , α_1 . The magnetic field H is applied to the segment ℓ and its direction is along the longitudinal axis of the fiber [2]. Since the linearly polarized beam is propagated serially through the fiber segments ℓ_0 , ℓ , ℓ_1 and the Wollaston prism we can obtain the formula for the final electric field intensities, E_1 & E_2 , through the construction of the input matrix of the linearly polarized light beam and a series of Jone's matrices for the fiber segments (ℓ_0 , ℓ , ℓ_1) and the Wollaston prism [26].

Rectangular coordinates are used in this approach where the x and y axes represent the fast and slow axis of the refractive index of the fiber respectively. Assuming the polarization direction of the linearly polarized input beam to be along the y axis the input matrix is as follows

$$\begin{bmatrix} 0 \\ E_0 \end{bmatrix} \quad (5.1)$$

where E_0 represents the initial electrical field intensity. The birefringence transmission character of the Hi-Bi optical fiber can also be expressed by a Jones matrix. In the fiber segments ℓ_0 and ℓ_1 the phase differences α caused by the birefringence are α_0 and α_1 respectively, and as there is no magnetic field applied to them their transmission matrices can

be expressed respectively by the following Jones matrices [27].

$$\begin{bmatrix} \exp(i\alpha_0/2) & 0 \\ 0 & \exp(-i\alpha_0/2) \end{bmatrix} \quad (5.2)$$

$$\begin{bmatrix} \exp(i\alpha_1/2) & 0 \\ 0 & \exp(-i\alpha_1/2) \end{bmatrix} \quad (5.3)$$

When the magnetic field H is applied to the segment ℓ of the fiber then the Faraday effect will be included in the Jones matrix [28]. It has been shown [2] that this can be accurately written as

$$\begin{bmatrix} \cos\theta + i\cos\zeta\sin\theta & -\sin\zeta\sin\theta \\ \sin\zeta\sin\theta & \cos\theta - i\cos\zeta\sin\theta \end{bmatrix} \quad (5.4)$$

where

$$\Theta = \Phi/2$$

$$\Phi = [\alpha^2 + (2\Omega)^2]^{1/2}$$

$$\alpha = B_F \cdot \ell$$

$$\Omega = V \cdot H \cdot \ell$$

$$\sin \zeta = 2\Omega/\Phi = \Omega/\Theta$$

$$\cos \zeta = \alpha/\Phi = \alpha/2\Theta$$

In above equations, B_F is the birefringence of the Hi-Bi fiber, α is the phase shift caused by the birefringence B_F in the optical fiber with length ℓ , Ω is the rotation angle of the linearly polarized beam propagating in the optical fiber with length ℓ under the influence of the magnetic field H [2].

In the Hi-Bi optical fiber, generally, we have $\alpha \gg \Omega$ [2], so that $\Phi \approx \alpha$, $\sin \zeta \approx 2\Omega/\alpha$ and $\cos \zeta \approx 1$. The Jone's matrix (5.4) can be simplified as follows

$$\begin{bmatrix} \cos(\alpha/2) + i\sin(\alpha/2) & -(2\Omega/\alpha) \cdot \sin(\alpha/2) \\ (2\Omega/\alpha) \cdot \sin(\alpha/2) & \cos(\alpha/2) - i\sin(\alpha/2) \end{bmatrix} \quad (5.5)$$

that is

$$\begin{bmatrix} \exp(i\alpha/2) & -(2\Omega/\alpha) \cdot \sin(\alpha/2) \\ (2\Omega/\alpha) \cdot \sin(\alpha/2) & \exp(-i\alpha/2) \end{bmatrix} \quad (5.6)$$

When the main axis of the Wollaston prism is at $\pm 45^\circ$ to the fast (or slow) axis of the fiber then its standard transmission [10] matrix can be expressed as:

$$\frac{1}{\sqrt{2}} \begin{bmatrix} 1 & 1 \\ -1 & 1 \end{bmatrix} \quad (5.7)$$

Based on the above matrices (5.1), (5.2), (5.3), (5.6) and (5.7), the expression for the final electric field intensities, (E_1, E_2) , output by the Wollaston prism is [2]:

$$\begin{aligned} \begin{bmatrix} E_1 \\ E_2 \end{bmatrix} &= \frac{1}{\sqrt{2}} \begin{bmatrix} 1 & 1 \\ -1 & 1 \end{bmatrix} \cdot \begin{bmatrix} \exp(i\alpha_1/2) & 0 \\ 0 & \exp(-i\alpha_1/2) \end{bmatrix} \cdot \\ &\cdot \begin{bmatrix} \exp(i\alpha/2) & -(2\Omega/\alpha) \cdot \sin(\alpha/2) \\ (2\Omega/\alpha) \cdot \sin(\alpha/2) & \exp(-i\alpha/2) \end{bmatrix} \cdot \\ &\cdot \begin{bmatrix} \exp(i\alpha_0/2) & 0 \\ 0 & \exp(-i\alpha_0/2) \end{bmatrix} \cdot \begin{bmatrix} 0 \\ E_0 \end{bmatrix} \end{aligned} \quad (5.8)$$

Note that the matrices must follow chronologically the order in which the different events are encountered. It has been shown [2] that Eq.(5.8) can be accurately rewritten as

$$|E_1|^2 = \frac{|E_0|^2}{2} \left[1 - \frac{4\Omega}{\alpha} \cdot \sin(\alpha/2) \cdot \cos(\alpha/2 + \alpha_1) \right] \quad (5.9)$$

$$|E_2|^2 = \frac{|E_0|^2}{2} \left[1 + \frac{4\Omega}{\alpha} \cdot \sin(\alpha/2) \cdot \cos(\alpha/2 + \alpha_1) \right] \quad (5.10)$$

Thus if $H = 0$, then $\Omega = 0$, so

$$|E_1|^2 = |E_2|^2 = \frac{|E_0|^2}{2} \quad , \text{ the initial set up condition.}$$

The light intensities detected by the photodetectors are [2]:

$$I_1 \propto |E_1|^2 \quad (5.11)$$

$$I_2 \propto |E_2|^2 \quad (5.12)$$

Finally we can obtain the output signal S in which the effect caused by any instability in the optical source output power is theoretically removed through the division

$$S = \frac{I_2 - I_1}{I_2 + I_1} \quad (5.13)$$

(Note: The effect of division will be discussed thoroughly in chapter 7.)

Combining equations (5.9), (5.10) and (5.11), (5.12), and substituting for I_1 , I_2 in equation (5.13), we get

$$S = 2\Omega \cdot \frac{\sin(\alpha/2)}{\alpha/2} \cdot \cos(\alpha/2 + \alpha_1) \quad (5.14)$$

From the above equation (5.14) it is seen that the output signal S is proportional to the Faraday rotation angle Ω . That is, S is proportional to the magnetic field intensity H applied to the fiber segment of length ℓ and also to the fiber length ℓ . If the magnetic field intensity H and its spatial distribution are kept unchanged, and letting the fiber length ℓ be a constant, then the phase shift α is also unchanged, so that $2\Omega \cdot (\sin(\alpha/2))/(\alpha/2)$ is a constant. If the magnetic field H is moved along the longitudinal direction of the fiber (z -axis), meanwhile keeping its intensity, spatial distribution and length ℓ unchanged, then the magnitude α_1 will change with the variation of the fiber length ℓ_1 because of the movement of the magnetic field H . The output signal S is thus modulated in cosine form, $\cos(\alpha/2 + \alpha_1)$. If the phase shift α_1 changes 2π and since $\alpha/2$ is a constant then the magnitude of the output signal S will change over that period. Thus the variation of the fiber length ℓ_1 , which causes the phase shift α_1 to change 2π , is defined as one beat length in the Hi-Bi

optical fiber [2]. By definition,

$$\delta = 2\pi/\ell_B \quad (5.15)$$

where δ is the birefringence and ℓ_B the beat length of the Hi-Bi optical fiber thus

$$\alpha_1 = \delta \cdot \ell_1 = 2\pi \cdot \ell_1 / \ell_B \quad (5.16)$$

The output signal S in equation (5.14) can be expressed as

$$S = A \cdot \cos(\alpha/2 + 2\pi \cdot \ell_1 / \ell_B) \quad (5.17)$$

$$A = 2\Omega \cdot \frac{\sin(\alpha/2)}{\alpha/2} = \text{constant} \quad (5.18)$$

The relationship between the output signal S and the fiber length ℓ_1 is determined from equation (5.17) and the beat length of the fiber obtained from this relationship is shown in Fig.5.2 [2].

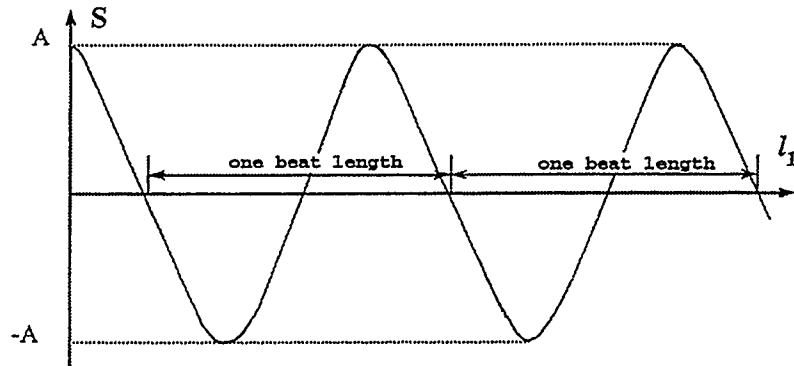


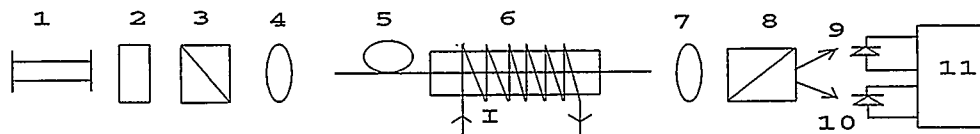
Fig.5.2 The relationship between the output signal S and the fiber length.

Thus moving the magnetic field to a position where $S = 0$,

taking this position as reference point, then moving the magnetic field until the magnitude of the output signal S goes through two zeros produces a phase shift α_1 exactly equal to 2π . The distance from this point to the reference point is exactly equal to one beat length of the fiber [2].

5.3 Implementation scheme

Fig.5.3 shows the initial experimental setup for measuring the beat length of the Hi-Bi fiber.



- 1- Laser 2- Quarter-wave plate 3- Polarizer
- 4- Plano-convex lens 5- Hi-Bi-fiber
- 6- Current coil to produce magnetic field
- 7- Micro lens 8- Wollaston prism
- 9 & 10- Photodiodes 11- Signal processing Unit

Fig.5.3 Initial experimental set-up.

The collimated light beam output by the laser is converted into a linearly polarized beam by the polarizer and it is then injected into the Hi-Bi fiber by the way of a plano-convex lens. A section of the fiber is then passed through the magnetic field produced by the current coil and a microlens is placed at the output end of the fiber to convert the diverging

beam into a parallel beam. This parallel output beam is then split into two beams by the Wollaston prism, each of these outputs being detected by a photo diode. In the signal processing unit the output signal S is obtained by an analogue circuit. The improvements in the initial setup will be given in chapter 6.

Chapter 6

Instrument Design

6.1 Basic Requirements

On the basis of the theoretical explanation of the proposed technique in chapter 5 an experimental set-up is built. A solid steel slab (1 mx 0.6m x 0.02m) is used for the initial experimental set-up in order to give a solid flat surface for the bases of the component holders. The following requirements were deemed to be necessary in order to obtain acceptable results

- a) an acceptable level of optical output power from the single-mode fiber,
- b) a strong magnetic field in order to obtain a measurable Faraday rotation,
- c) sufficiently sensitive detection circuitry and,
- d) a vibration-isolated optical system set-up.

The following is the detailed explanation for the above four requirements.

6.2 Coupling the optical power into the fiber

An acceptably high level of power out of the fiber is required in order that the detection circuit operates well above the noise level. The maximum optical power can be coupled into the

fiber as long as it has a well cleaved input facet and the appropriate lens system is well aligned. The first fiber to be used was Newport's Hi-Bi F-SPV. This SMF has cladding/coating diameter of 125/250 μm , nominal core diameter of 2.6 μm , mode field diameter of 3 μm - 3.4 μm , cutoff wavelength of 550nm and a typical beat length of 2.0mm at the operating wavelength of 633nm [29].

Good expertise is required to achieve a well cleaved fiber input and output facet. The cleaving of the fiber starts with the removal of the buffer jacket. Initially this task is done by hand but a lot of fiber is wasted due to breakage since the glass fiber is relatively fragile. Later on, upon the advice of the fiber manufacturer, paint stripper is used to soften the plastic buffer and ease its removal.

Two methods are used to cleave the fiber. Firstly, the fiber is cleaved by softly touching the sapphire cleaver blade on the fiber cladding and then the cleaved piece is snapped off. The second way to cleave the fiber is to wrap the 3cm end piece of the fiber around a finger, to introduce tension on the fiber, and then just by touching the cleaver blade on the surface of the fiber cladding it will cleave itself. Both methods provide well cleaved fiber facet but it is found that the first method generally produces better results and is relatively easy after a little practice. The other end of the fiber is also cleaved in the same manner. The two ends of the fiber are then checked by microscope to ensure that the

end-faces or facets of the fiber are properly cleaved and clean. A typical illustration of an end-face is given in Fig.6.1.

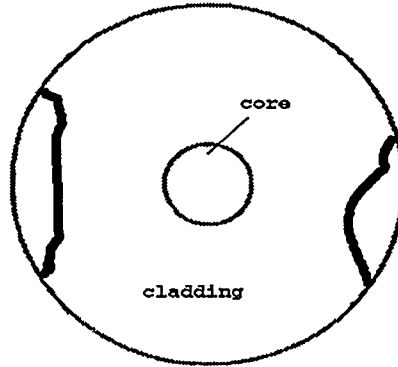


Fig.6.1 Cleaved fiber facet.

It can be noted from Fig.6.1 that the outer portion of the end-face (the cladding) is not necessarily perfectly smooth but the core has a very good cleave. This is one advantage of the single mode fiber since it has a small core and large cladding it helps to obtain better results.

The next step is to couple the maximum power into the fiber and this is done by using the appropriate lenses and alignment system. Since the fiber core diameter is $2.6\mu\text{m}$, which is smaller than the core diameter of conventional single-mode fiber (normally $> 6\mu\text{m}$), the selection of the appropriate lens is done on the basis of their spot size which can be calculated by [17]

$$\text{Spot size } d = 1.22 \lambda f/\# \quad (6.1)$$

where λ is the free space wavelength and $f/\#$ is the f-number of the lens. The f-number is also called the lens speed or

light gathering ability of the lens and it is equal to the focal length of the lens divided by lens diameter. So the spot size of the plano-convex lens (Mells-Griot # 01LPX198), which is used to focus the He-Ne laser beam of 5mw optical power, is calculated by

$$d = 1.22 * 632.8\text{nm} * 4.2 = 3.2\mu\text{m}.$$

This spot size is still larger than the core diameter of fiber (2.6 μm) so the laser beam could not be properly injected into the fiber and hence an optical power of 10 μw obtained at the output of the fiber was insufficient. A microscope objective (X10) is then used to focus the laser beam and the spot size is calculated by using

$$d = 1.22 * 632.8\text{nm} * 0.13 = 0.1\mu\text{m}$$

As the spot size of the microscope objective is smaller than the core diameter it is used to focus the laser beam and an optical power of 560 μw is obtained at the output of the fiber. Since the f-number is a function of focal length and it is difficult to set a focal length of a few milli-meters, the spot size of the microscope objective does not actually equal the calculated size. Also the X-Y-Z translation used to position the fiber end is not particularly precise, but as the optical power obtained by the microscope objective is large , that is 560 μw , it is sufficient for the experiment.

6.3 Magnetic head design

The key consideration relating to this experimental

measurement system is the procedure for applying the magnetic field to the fiber. From equation (5.14), it is seen that the measurement sensitivity will decrease when $(\sin(\alpha/2))/(\alpha/2)$ is less than 1. In order to keep the measurement sensitivity at an acceptable level, we should have $(\sin(\alpha/2))/(\alpha/2) \geq 0.2$, and the value of phase difference α should be less than $3\pi/2$. Thus according to equation (5.16) the fiber region ' ℓ ' acted on by the magnetic field should be less than three quarters of one beat length ℓ_b . It is not very difficult to make the fiber region ' ℓ ' acted on by the magnetic field to be less than a few millimetres by using a magnetic air gap, and a fiber beat length which is in the millimetre range can then be measured [2].

In addition, from equation (5.18), it is found that the measurement sensitivity is proportional to the Faraday rotation angle Ω , that is, the Verdet constant ' V ', the magnetic field intensity ' H ' and the length of the fiber which it acts upon, ' ℓ '. Since the Verdet constant of the fiber is very small (0.016min/Amp), the magnetic field intensity must be strong enough when the magnetic gap width is about one millimetre [2]. The next key objective of this project is to design a magnetic head with a sufficiently large magnetic field intensity ' H '. The geometrical shape of the designed magnetic head with its air-gap is shown in Fig.6.2.

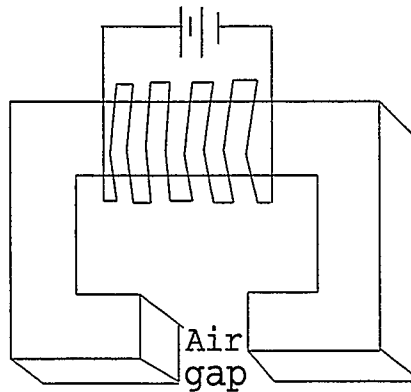


Fig.6.2 Magnetic head with air-gap.

According to Zhang [6], a magnetic field intensity of 3000 Gauss should be sufficient for the purpose of this experiment so a magnetic head of 3000 Gauss was designed.

It was observed that a magnetic field intensity of 3000 Gauss was insufficient to give an easily measurable Faraday rotation so it was decided to build a magnetic head with a larger core to increase the magnetic field intensity. To achieve this purpose a square core of soft-steel casting with a mean length ' l_i ' of 63.52cm, a cross-sectional area ' S_i ' of $6.25 \times 10^{-4} \text{cm}^2$ (2.5cm x 2.5cm) and an air-gap of ' l_a ' 1.2mm were chosen for the new magnetic head. In order to produce a magnetic field intensity of 6000 Gauss (or 0.6 Tesla) in the air-gap the number of turns of copper wire required with a current of 10 amperes had to be calculated (since only two 6 Amperes supplies were available). The calculations are as follows:

$$\Phi = B * S_i = 0.6 * 6.25 \times 10^{-4}$$

$$= 3.75 * 10^{-4} \text{Wb.}$$

From the B-H curve in the appendices for soft steel, for $B = 0.6$ Teslas, $H = 300$ ampere-turns/m, so ampere-turn for the core is

$$\begin{aligned} F_i &= H_i * \ell_i = 300 * 63.52 * 10^{-2} \\ &= 190.56 \text{A-T.} \end{aligned}$$

Area of the air-gap

$$S_a = (0.025 + 0.0012)^2 = 6.8644 \times 10^{-4} \text{ m}^2.$$

Ampere-turn for the air-gap is

$$F_a = H_a * l_a = \frac{\phi * l_a}{\mu_0 * S_a} = \frac{3.75 * 10^{-4} * 1.2 * 10^{-3}}{4\pi * 10^{-7} * 6.8644 * 10^{-4}} = 521.67 \text{A-T}$$

$$F = F_i + F_a = 190.56 + 521.67 = 712.23 \text{A-T}$$

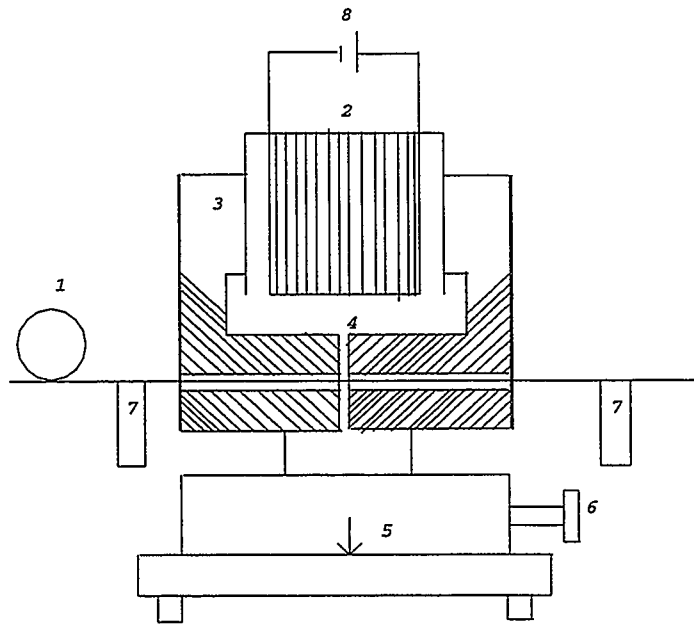
So, for 10 amperes, the number of turns required,

$$N = F/I = 712.23/10 \approx 71 \text{ turns}$$

So 71 turns of wire AWG-16 (current rating = 13 A) with 10 amperes current will produce a magnetic field intensity of 6000 Gauss in a 1.2mm air gap. The normal air gap was about 1.5mm but it was squeezed to 1.2mm with a large C-clamp. The magnetic field intensity was measured with a BELL-110 Gauss meter.

A hole of 2mm diameter was drilled horizontally through the head for the passage of the fiber and the magnetic head then fixed to a moving assembly. The moving assembly was then used to move the head and thus the magnetic field along the

fiber. The magnetic head could be moved in increments of 0.5mm with the help of a micrometer attached to the moving assembly. Due to the relatively fast drift in the values of I_1 and I_2 , as a result of the optical source instability, and also due to some 'stickiness' (lack of smooth travel) in the head moving assembly translation stage, it was determined that the optimum displacement step size was 0.5mm. Fig.6.3 illustrates the magnetic head attached on to the moving assembly.



- | | |
|--|-------------------|
| 1- The Hi-Bi fiber to be measured | |
| 2- Current coil used to produce magnetic field | |
| 3- The magnetic core | 4- The air gap |
| 5- The head moving assembly | 6- The micrometer |
| 7- Fiber stand/holder | 8- supply to coil |

Fig.6.3 The magnetic head with moving assembly.

6.4 Signal processing unit

The output beam from the fiber was 'collimated' by means of a micro lens and focused onto the Wollaston prism which then split it into two beams. These two beams can be observed as two bright spots at the output of the Wollaston prism. The change in the intensity of the two spots at the output of the Wollaston prism due to the Faraday rotation (that is when the magnetic field was applied) had to be measured opto-electronically. The signal processing unit which did this job consisted of two parts 1) Matched photo-diodes, also called the Bi-cell, and 2) the processing circuit for the two photodiode output signals.

A crucial part of this phase was to be able to focus the Wollaston prism output beams onto the tiny matched photodiodes. The active area of each photodiode was 1.3mm^2 thus a spot size of less than 1.3mm^2 was required to completely focus the two beams onto their respective photodiodes. A micro-lens (Oriel # 40209) of f-number 1.3 was used to 'collimate' and focus the output beam from the fiber onto the Wollaston prism which then produced the two output beams. The spot size for this micro-lens can be calculated as

$$d = 1.22 * \lambda * f/\# = 1.22 * 632.8\text{nm} * 1.3 = 1\mu\text{m}$$

This spot size was small enough to produce two tiny spots of only a few micrometers in diameter after the Wollaston prism, which was then easily focused onto the Bi-cells. Note that the

outputs of the Wollaston prism are not truly collimated beams. The Bi-cell used (ECG # UV 100BG dual) has a peak responsivity of 0.44 A/W at 632nm wavelength and its typical spectral response is given in the appendices.

The signal processing circuit of ref. [24] was used in the initial stages of this project. This circuit is based on a dual path detection and measuring method [24] that eliminates the intensity-dependence of the Faraday signal. The schematic representation of the dual path measuring method is shown in Fig.6.4.

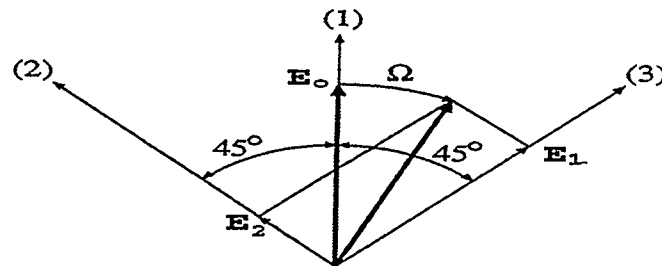


Fig.6.4 Schematic representation of the dual path measuring method.

In this method [24] the Wollaston prism splits the linearly polarized light into two diverging beams as shown in Fig.6.4. The state of polarization of the incident light (1) (amplitude E_0 , intensity J_0 which is proportional to the square of amplitude E_0) contains the transmitted states of polarization (2) and (3) of the Wollaston prism, each of them being at an

angle of 45° to \mathbf{E}_0 . The component beams (amplitudes \mathbf{E}_1 and \mathbf{E}_2 with intensities J_1 and J_2 respectively) polarized orthogonal to each other are intercepted by the two photo detectors (bi-cells). Assuming the transmitting directions of the Wollaston prism outputs to be $\pm 45^\circ$ then the component electric fields \mathbf{E}_1 and \mathbf{E}_2 at the Wollaston prism output are

$$\mathbf{E}_1 = \mathbf{E}_0 \cos(45^\circ - \Omega) \quad (6.2)$$

$$\mathbf{E}_2 = \mathbf{E}_0 \cos(45^\circ + \Omega) \quad (6.3)$$

Thus the corresponding component beam intensities J_1 and J_2 detected by two photo detectors are

$$J_1 = |\mathbf{E}_1|^2 = |\mathbf{E}_0|^2 \cos^2(45^\circ - \Omega)$$

$$J_1 = \frac{|\mathbf{E}_0|^2}{2} [1 + \cos(90^\circ - 2\Omega)]$$

since $J_0 \propto \mathbf{E}_0$, J_1 will be

$$J_1 = \frac{J_0}{2} [1 + \sin 2\Omega] \quad (6.4)$$

$$\text{Similarly } J_2 = |\mathbf{E}_2|^2 = |\mathbf{E}_0|^2 \cos^2(45^\circ + \Omega)$$

$$= \frac{|\mathbf{E}_0|^2}{2} [1 + \cos(90^\circ + 2\Omega)]$$

From Eq.(6.4) and Eq.(6.5), we can derive a signal as follows

$$S = C \cdot \left(\frac{J_2 - J_1}{J_1 + J_2} \right) = C \cdot \sin 2\Omega \quad (6.6)$$

which is theoretically independent of the input light

$$\text{thus } J_2 = \frac{J_0}{2} [1 - \sin 2\Omega] \quad (6.5)$$

intensity J_0 . 'C' is a constant voltage inherent in the analog electronic circuit which is performing the division [24]. The dual path detection scheme shown in Fig.6.5 realizes the above arithmetic operation [24].

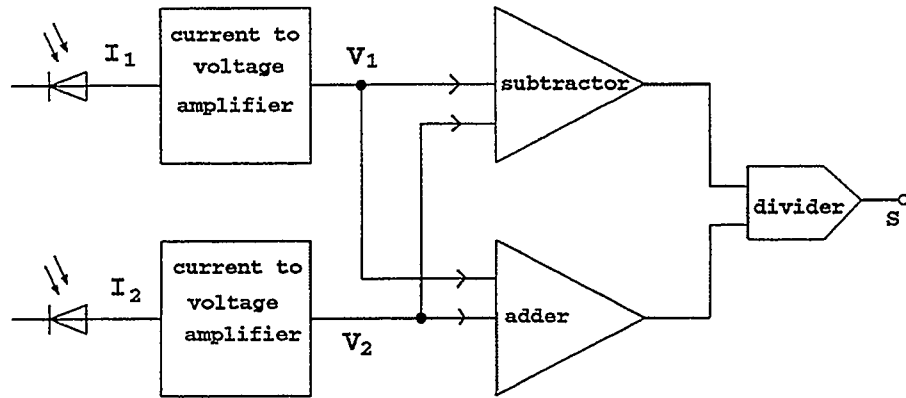


Fig.6.5 Schematic representation of dual path detection.

Fig.6.6 illustrates the detection unit which consists of the silicon Bi-cell photo-detector and the analog circuits (current-voltage amplifiers, subtractor and adder). In order to maintain the measurement accuracy to a high degree the two photo-diodes and the dual path should be essentially identical which is why a silicon Bi-cell photo-detector is used instead of two individual photodiodes and all the opposite electronic components in the dual path are virtually identical. Fig.6.6 shows the detection circuit with the identical opposite components [24].

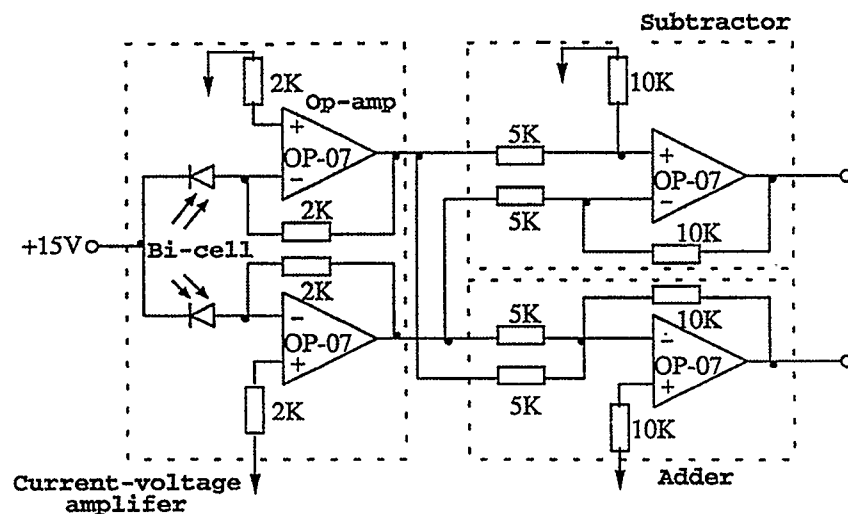


Fig.6.6 The photo-detection and signal processing circuit.

It was concluded that the subtraction alone of the two Wollaston prism output signals could serve the purpose of this project though the division of the difference by the sum of the two signals was also considered since it should have

compensated for the effects of any variations in the output signal due to laser output power fluctuations, electronic circuit imbalances etc. It was however observed that the division process did not compensate for these errors in our experiments. This will be discussed thoroughly in chapter 7.

The electronic circuit used by ref. [24] was built on a breadboard, unshielded and not properly grounded. These factors introduced a great deal of noise to the low power output signal and it was observed that the output signal could be very unstable. It was found that when the same circuit was built on a printed circuit board (PCB) and properly grounded and shielded that the noise level was reduced very significantly. Table 6.1 shows the improvement in the results.

Nodes -----	Node	Node	Node	Node
RMS noise voltage(μ v)	V_1	V_2	$V_1 + V_2$ (Addition)	$V_2 - V_1$ (Subtraction)
Ref. [10] circuit.	1.00	1.00	1.45	100
New circuit	0.75	0.75	1.20	1.9

@ 1KHz frequency and 300Hz bandwidth.

Nodes V_1 and V_2 are shown in Fig.6.5.

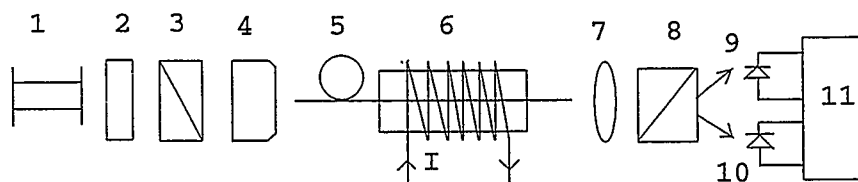
Table 6.1 Noise factor improvement results.

The results in Table 6.1 were measured with a Hewlet-Packard wave analyzer (#3581 A). It can be noted from Table 6.1 that the noise factor at the subtracter output improved

significantly and this in turn helped greatly in the measurement of the very small change in the output signal due to the Faraday effect. Since the division process did not help at all (discussed in chapter 7), the subtracter output was used for all observations and results.

6.5 Assembling the instrument

On the basis of above theory, calculations and discussion, an experimental set-up for measuring the beat length in the Hi-Bi fiber was assembled as shown in Fig.6.7.



- 1- Laser 2- Quarter-wave plate 3- Polarizer
- 4- Microscope objective 5- Hi-Bi fiber
- 6- Current coil to produce magnetic field
- 7- Micro lens 8- Wollaston prism 9 & 10- Photodiodes
- 11- Signal processing unit.

Fig.6.7 The experimental measuring system.

In this 'proof-of-concept' experiment, a linearly polarized light beam from the laser is passed through a quarter-wave ($\lambda/4$) plate and then a rotatable polarizer. The orientation of the $\lambda/4$ plate is adjusted to give circularly

polarized light so that the intensity of the linearly polarized light after the polarizer is independent of the polarization angle [7]. The resulting beam is focussed onto the prepared end-face of a sample of Polarization Maintaining single-mode optical fiber using a X10 microscope objective. The small diameter of the core means that, inevitably some of the light is also launched into the cladding. This light is removed by two techniques. Firstly an attempt is made to remove the cladding light by stripping the buffer jacket off a 5cm portion of the fiber and than bending it so that the cladding light would escape through the stripped part. This scheme did not give a sufficiently significant improvement. Secondly an index matching liquid is then applied to the stripped section of the bent part of the fiber and it produced the desired results. A section of the fiber is then passed through the magnetic head in order to apply the magnetic field to a specific part of the fiber. A micro-lens is placed at the output end of the fiber to convert the diverging output beam into an approximately collimated beam. Index-matching liquid is also used at the output end of the fiber to remove any cladding light that might have been induced in the cladding due to reflections or scattered light. The focused beam is then split into two angularly displaced beams with orthogonal linear polarizations by the Wollaston prism and the intensities of the two beams I_1 and I_2 are detected by the Bi-cell. The Bi-cell is coupled to the analog circuit (the

combination being called the detection circuit) which computes the function

$$S = \frac{I_2 - I_1}{I_1 + I_2} \quad (6.7)$$

where S is the output signal. However the denominator of Eq.(6.7) is not used due to the reasons to be described in chapter 7.

Assembly of the beat length measuring instrument requires a great deal of care and sensitive handling. The alignment of the system components requires much attention since focusing and power coupling into the single-mode fiber is very critical for good results. The fiber must be handled carefully since it is relatively fragile. Also the laying down of the fiber on the work table must be done carefully since small bends, twists and tape-pressure can affect birefringence and the state of polarization [6]. This relatively stable system is then used to obtain reasonably acceptable experimental results (initially the set-up is established on a solid steel slab). After obtaining the initial experimental results (described in chapter 7), the set-up is transferred onto a vibration-isolation table in order to achieve improved results. The details of these improvements will be discussed thoroughly in chapter 7.

Chapter 7

Observations and results

The experimental set-up shown in Fig.6.7 was used to implement this 'proof of concept' project and the beat length of four different fibers were measured. Table 7.1. gives the manufacturer specified data for the four fibers measured.

Fibers/Data	F-SPV	F-SPA	F-SPM	F-SPZ
Cladding/Coating dia. (μm)	125/250	125/250	81/206	80/200
Mode field Dia. (μm)	3.0-3.4	2.74-3.0	5.4	5.6
Nominal core dia. (μm)	2.6	1.9	N/A	N/A
Numerical aperture (NA)	0.16	0.11	N/A	N/A
Operating wavelength (nm)	633	514	820	820
Cutoff wavelength (nm)	550	400	700	750
Beat length (mm)	2.01	2.0	1.02	0.88

F-SPV and F-SPA are from Newport Inc;

F-SPM and F-SPZ are from 3-M Inc;

Table 7.1 Data of fibers used in experiment.

Using the visible He-Ne laser beam eases the alignment and focussing challenges therefore the Beat length in fibers F-SPV and F-SPA were measured first since they have operating

wavelengths (632nm and 514nm respectively) in the visible band. As fibers F-SPM and F-SPZ have their operating wavelengths (820nm) in the invisible band an infra-red (IR) detection card (Kodak # 27523Z) was used to detect and focus the invisible laser beam produced by the GALA laser.

7.1 Experimental procedure and initial results

Since the original signal processing unit (SPU) of ref.[24] gave unstable and very difficult to record results due to the noise (as shown in Table 6.1), the initial experimental results were obtained using power meters since they made it easier to record the data. The initial experimental set-up is shown in Fig.7.1. Great care is taken so that the fiber did not touch the walls of the 2mm diameter hole in the magnetic head as it passed through it otherwise it may have caused vibration induced errors in the readings. The fiber is mounted carefully on the fiber holder and the magnetic head moved in 0.5mm increments with the readings recorded manually after each move. Two power meters (ANDO# AQ-2101) were used to detect the intensity variations in the two output beams after the Wollaston prism. The first set of results were obtained with no magnetic field applied to the fiber. A set of 20 readings were obtained and plotted using a spread sheet (LOTUS-123).

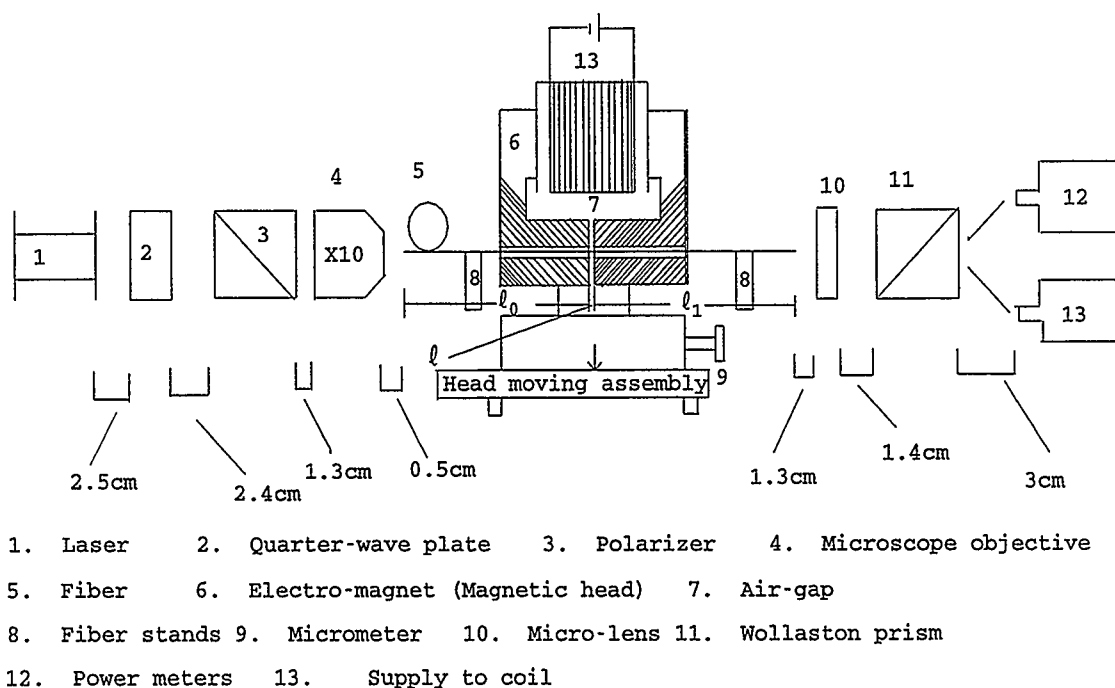


Fig.7.1 The beat length measuring system set-up showing distances between components.

Below are the plots of the initial results with no magnetic field applied to the fiber. This set of readings is important in order to observe the difference in plots when a magnetic field is applied. It can be observed from the Figs.(7.2 and 7.3) that no particular pattern is generated with no magnetic field applied. This means that the light intensities are unaffected by the head movement since the Faraday effect is not present. The fluctuations in the power meter readings (P_1 and P_2) are due mainly to source power fluctuation and vibrations in the system.

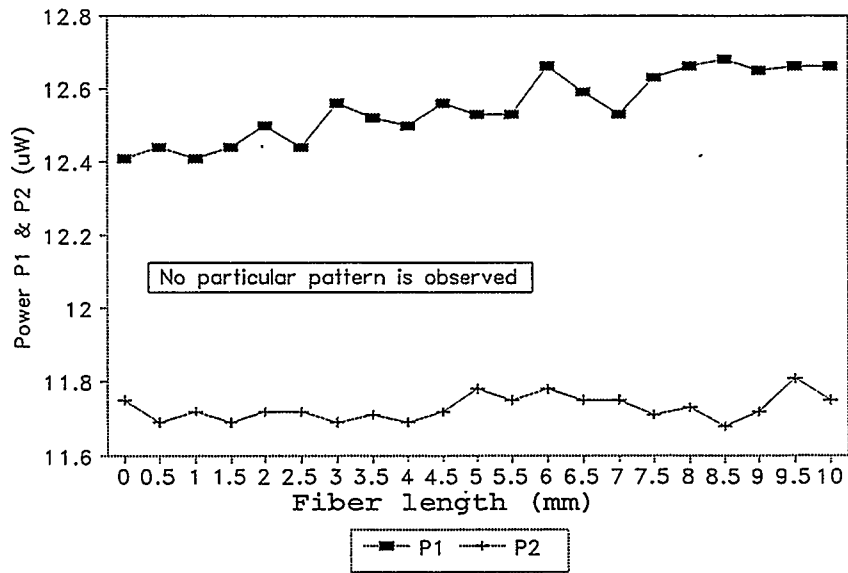


Fig.7.2 Fiber F-SPV @ 632 nm with no magnetic field applied.

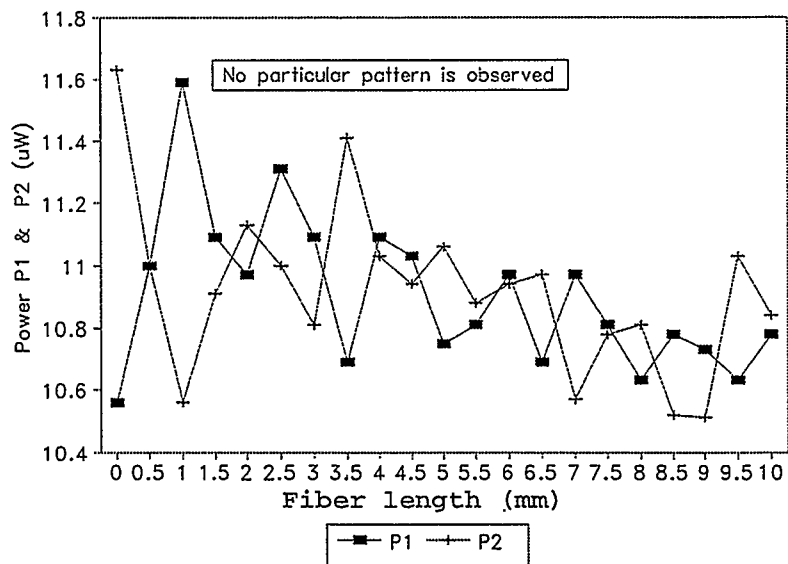


Fig.7.3 Fiber F-SPV @ 632 nm with no magnetic field applied.

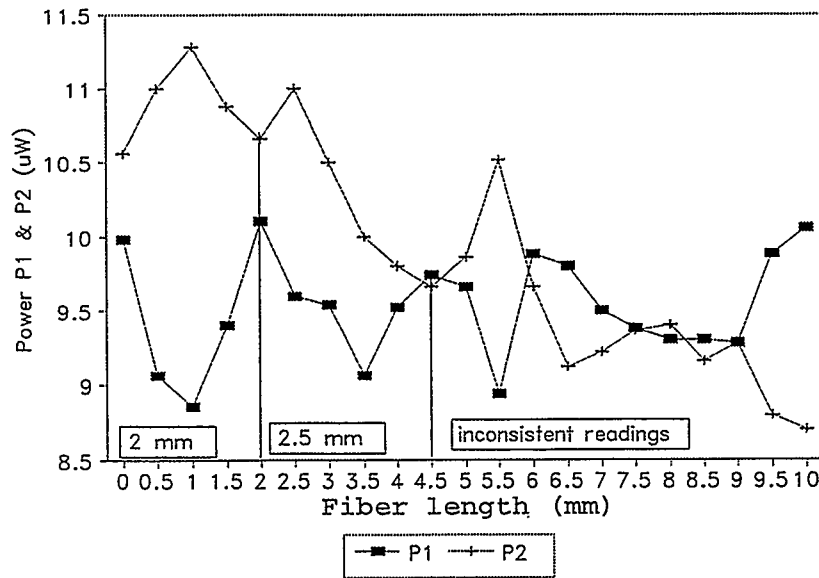


Fig.7.4 Beat lengths measured in F-SPV @ 632nm with (DC) magnetic field.

The next set of results were obtained with the magnetic field applied to the fiber. The magnetic field is produced by connecting a 6A DC supply to the magnetic coil. The magnetic field is moved along the fiber F-SPV in 0.5mm increments using the micrometer that is mounted on the head moving assembly and the readings were recorded manually after each move. Due to the relatively fast drift in the values of P_1 and P_2 , as a result of the optical source instability, and also to some 'stickiness' (lack of smooth travel) in the head moving assembly translation stage, it was determined that the optimum incremental step size was 0.5mm. Due to the Faraday effect the power in the two beams varied after the Wollaston prism and this was recorded by two power meters. Figs.(7.4 & 7.5) show the initial results for the fiber F-SPV.

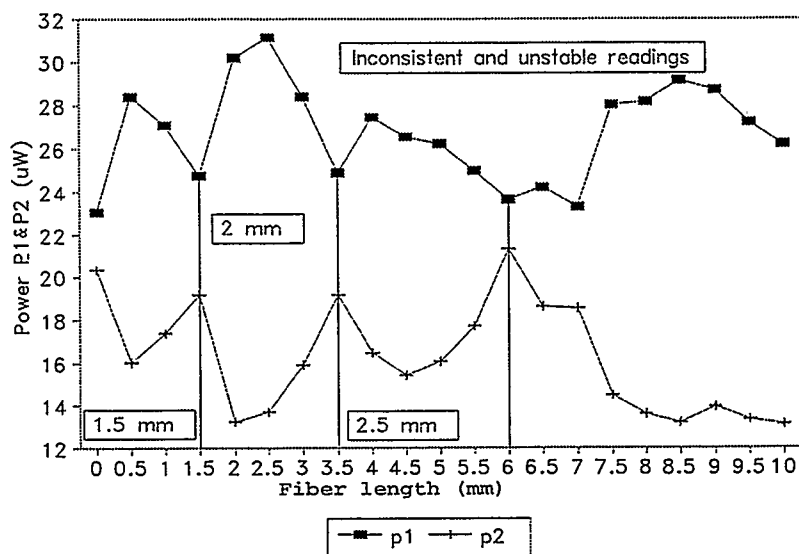


Fig.7.5 Beat lengths measured in F-SPV @ 632nm with (DC) magnetic field.

Eq.(6.7) is used to explain the obtained results, that is, the intensities of the two beams were subtracted and a beat length is obtained. Fig.(7.5) shows a number of beat lengths. A comparison of the Figs.(7.2 and 7.3) with Figs.(7.4 and 7.5) shows the variations in the intensities due to the Faraday effect. It is concluded that Figs.(7.4 and 7.5) strongly indicate the presence of a measurable beat length but that the results are relatively inconsistent.

Figs.(7.6 and 7.7) were obtained using an A.C. magnetic field to observe its effects on the Faraday rotation. It can be observed from the Figs.(7.6 and 7.7) that due to the relative weakness of the A.C. magnetic field there is less variation in the intensities of the two beams after the Wollaston prism. 60Hz vibrations in the magnetic core may also

be disturbing the readings. It was therefore decided that all future experimental results would be obtained using the D.C. magnetic field.

The same procedure was adopted to measure the beat length of fiber F-SPZ. This fiber has an operating wavelength of 814nm when using the IR laser (GALA). The results for F-SPZ are shown in Figs.(7.8 and 7.9). Since Faraday rotation is inversely proportional to wavelength, as shown in Fig.(7.10) [25], it can be seen from the Figs.(7.8 and 7.9) that the variations in the intensities of the two beams are significantly smaller at the wavelength of 814nm than for 632nm.

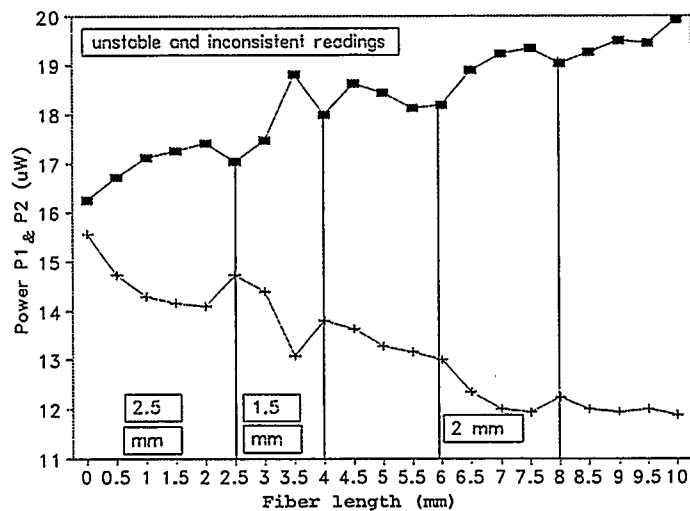


Fig.7.6 Beat lengths measured in F-SPV @ 632nm with (AC) magnetic field.

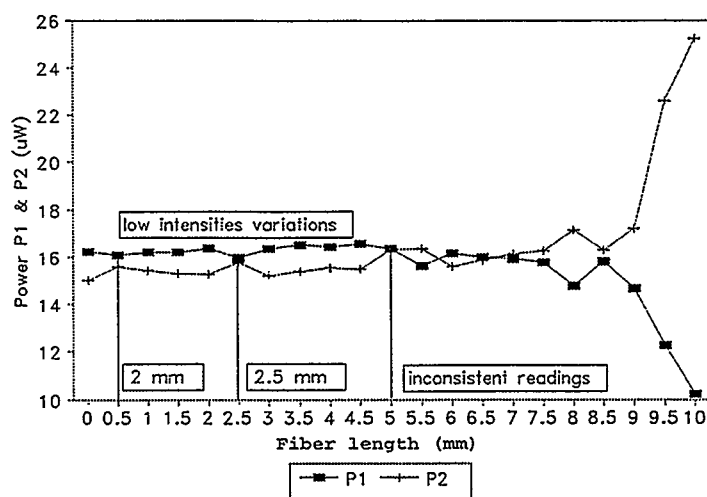


Fig.7.7 Beat lengths measured in F-SPV @ 632nm with (AC) magnetic field.

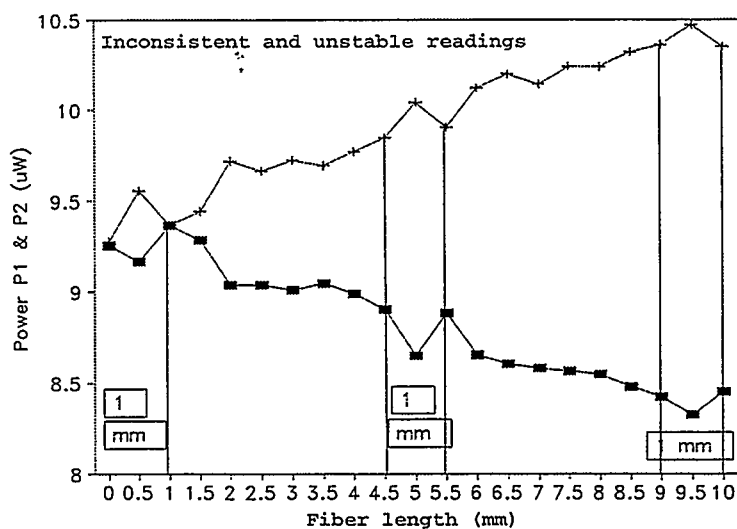


Fig.7.8 Beat length measured in F-SPZ @ 814nm with (DC) magnetic field.

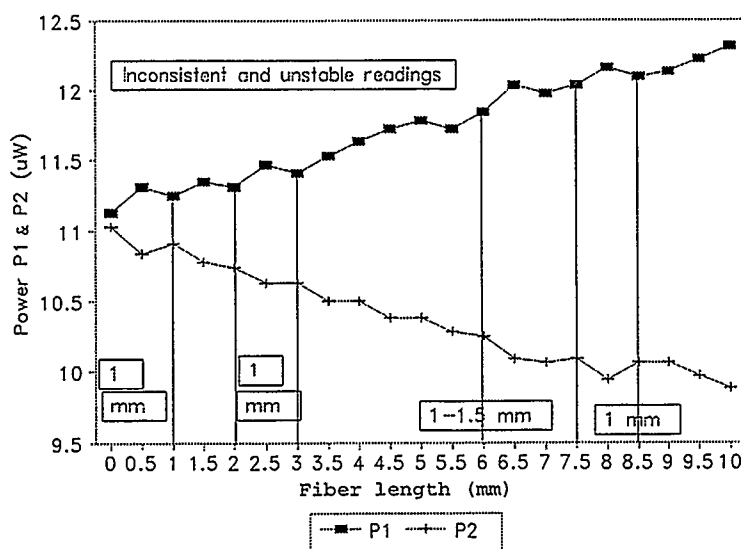


Fig.7.9 Beat lengths measured in F-SPZ @ 814nm with (DC) magnetic field.

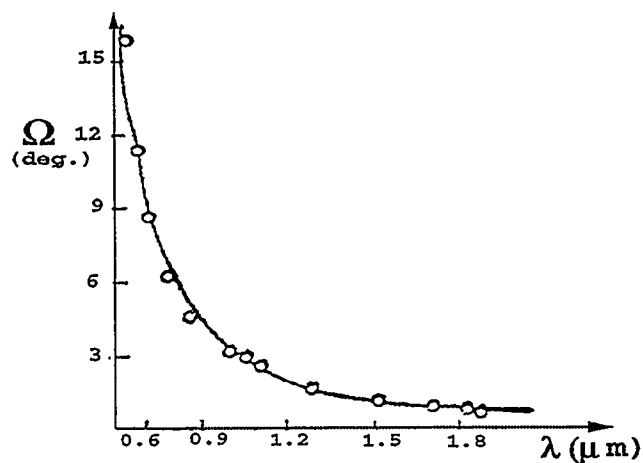


Fig.7.10 Faraday rotation Ω vs wavelength.

7.2 The sources of error and their corrections

It can be seen from the Figs.(7.4 to 7.9) that the results are rather questionable after one or two beat lengths. After a thorough review of the experimental setup, the

following factors are considered to be the main sources of error in the results.

1. Mechanical:

- a) Head moving assembly disturbances.
- b) Fiber vibrations.
- c) Power equipment vibrations.
- d) Ceiling fan air flow.
- e) Vibration of building.

2. Electrical:

- f) Magnetic head vibrations.
- g) Unshielded circuit - prone to noise.
- h) Circuit component noise.
- i) Circuit on bread board.
- j) Power supply ripples.
- k) Laser output power instability.

Most of the above problems were rectified using simple methods. The electro-magnet (head) was reattached to the head moving assembly much more securely in order to rectify problem (a). For (b) the fiber under very slight tension was firmly fixed to two very solid steel posts (2"x2"x4") at the entry and exit sides of the electro-magnetic head and this prevented any significant lateral movement of the fiber. For (c) the power equipment is transferred to a separate table to avoid the power equipment vibrations. For (d) the fiber vibrations due to ceiling fan air is stopped by closing off the fan air path. Problem 'e' is fixed by moving the experimental set-up onto a

vibration-isolated table. In (f) the AC magnetic field is produced by the AC supply that contributed vibrations to the magnetic head. Since the AC magnetic field produced a weak Faraday effect its use was abandoned and only the DC field used to obtain further results.

Problems (g), (h), and (i) had collectively a very significant and detrimental effect on the results and were very largely corrected by developing a printed circuit board (PCB) for the signal processing unit. Dual-sided PCB was used in order to use one side for common grounding and the other side for component mounting. The PCB was then shielded in an aluminium box and the outputs from this circuit were taken via shielded wire. These methods significantly reduced the noise as shown in Table 6.1. This procedure helped a great deal to get improved results and it will be discussed in section (7.3). For (j) the power supply ripples were reduced by switching to a precision power supply (Power Design Inc; Model # 2005). Problem (k) was very significant since the He-Ne laser output power would vary as much as 8% the GALA laser diode about 1%, as shown in Figs.(7.12 and 7.13). Source instability of less than 1% is generally considered to be acceptable.

It is claimed by many authors [10] that source instability can be compensated for by the operation $(I_2 - I_1)/(I_1 + I_2)$, but we have not found this to be the case as shown in Fig.7.12. One possible reason for this lack of

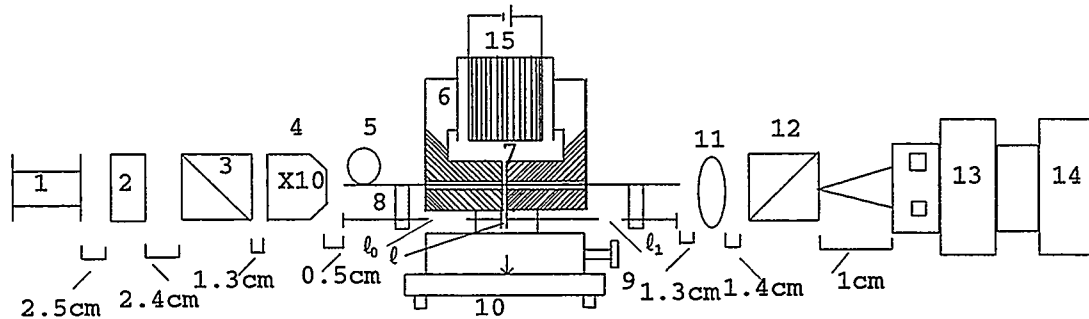
compensation is that the difference signal ($I_2 - I_1$) is very, very much smaller than the sum signal ($I_1 + I_2$) so that the division process is largely ineffective. In Fig.7.12 it can be observed that the division signal curve is exactly the same shape as the subtraction signal curve. A He-Ne laser of 1mW (Mells-Griot #05LHP111) with stabilizer was used to reduce the source fluctuations, but it is found that this source also had a power variation up to 5%, as shown in Fig.7.13. The source power variations is considered to contribute significantly to errors in the results shown in Table.7.2.

7.3 Intermediate results

After fixing the problems given above, intermediate results were recorded by the set-up shown in Fig.7.11, this set-up being placed on the vibration-isolated table. Careful alignment and focusing gave an adequate power at the output of the fiber that is, 500 μ W output from 4mW input. The shielded signal processing unit (SPU) was used instead of the power meters and the outputs from the electronic circuit were connected to the oscilloscope using shielded wire.

As the source fluctuation unstabilized the output signals I_1 , I_2 , ($I_2 - I_1$) and ($I_1 + I_2$), a storage oscilloscope was used to freeze each reading before recording it. The Y-axis on the Figs.(7.12 to 7.32) shows the intensities I_1 and I_2 of the two beams converted to voltages using the SPU. Figs.(7.12 and 7.13) show the results for the fiber F-SPV

at 632nm with DC magnetic field.



- 1- laser 2- Quarter-wave plate 2- polarizer
 3- microscope objective 5- fiber 6- electro-magnet(head)
 7- air gap 8. Fiber stands/holders 9- micrometer
 10- head moving assembly 11- micro lens
 12- Wollaston prism 13- signal processing unit (SPU)
 14- oscilloscope 15- DC supply to coil.

Fig.7.11 The final experimental set-up.

The significant improvement in the beat length measurement can be observed from Figs.(7.12 to 7.32) as compared to Figs.(7.3 to 7.9). Next the fiber F-SPA was placed in the system to measure its beat length and the results are shown in Figs.(7.14 and 7.15). Note that the experimentally obtained beat length of the F-SPA is greater than the manufacturers specified value since its nominal operating wavelength is 514nm in this case and a 632nm laser was used instead. The fiber beat length is increased by increasing the wavelength.

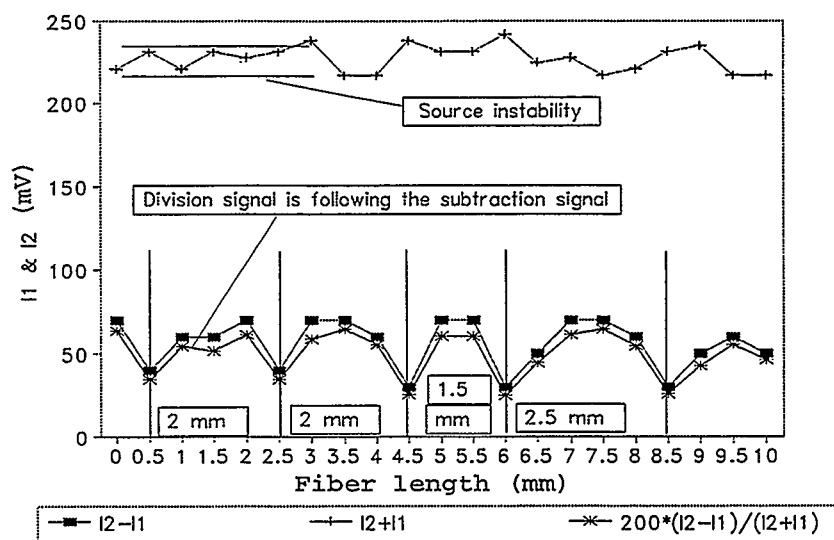


Fig.7.12 Beat lengths measured in F-SPV @ 632nm with (DC) magnetic field.

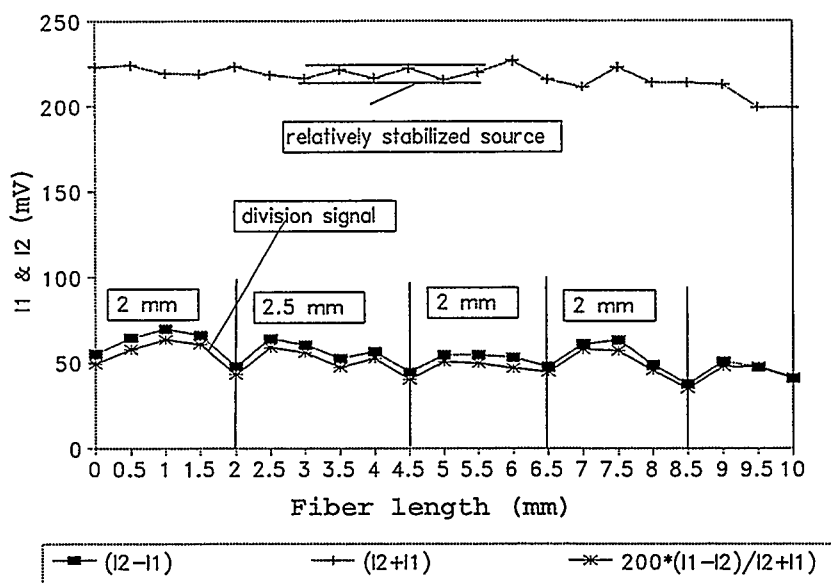


Fig.7.13 Beat lengths measured in F-SPV @ 632nm with (DC) magnetic field.

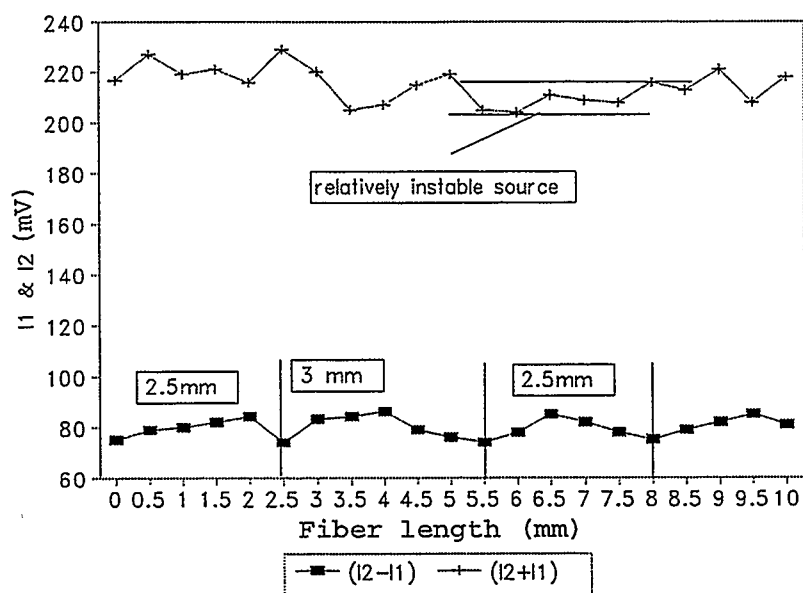


Fig.7.14 Beat lengths measured in F-SPA @ 632nm with (DC) magnetic field.

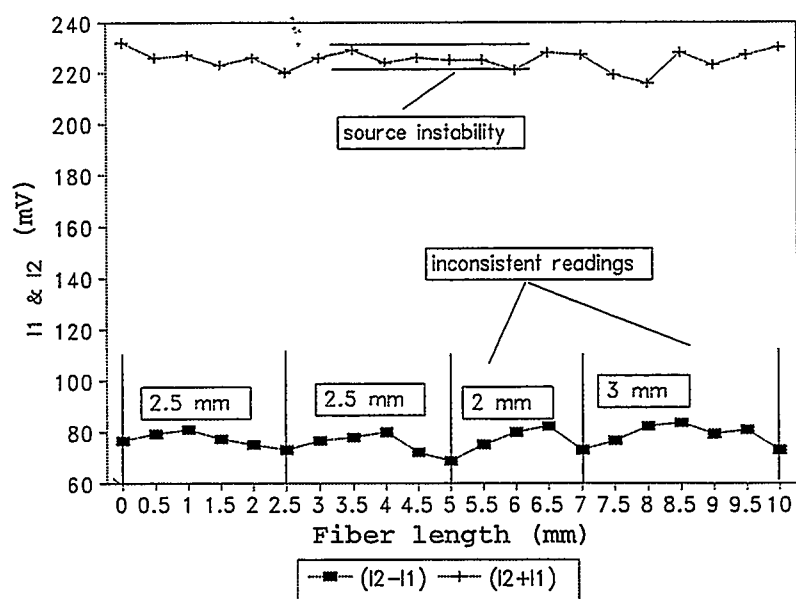


Fig.7.15 Beat lengths measured in F-SPA @ 632nm with (DC) magnetic field.

The fiber F-SPM was then placed in the system and since the nominal operating wavelength for this fiber is 820nm the GALA laser diode was used. Since this laser beam is invisible the alignment and focusing were done by using the infra-red detection card. Figs.(7.16 and 7.17) show the beat lengths obtained for this fiber.

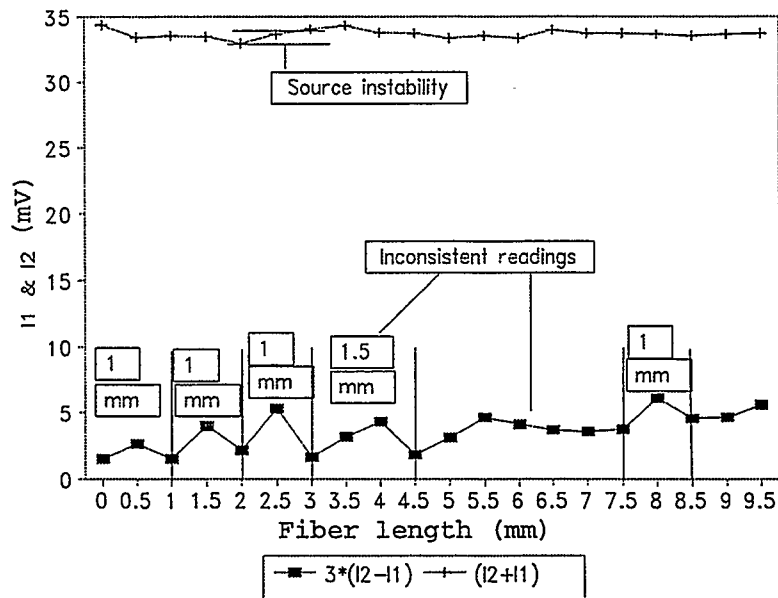


Fig.7.16 Beat lengths measured in F-SPM @ 814nm with (DC) magnetic field.

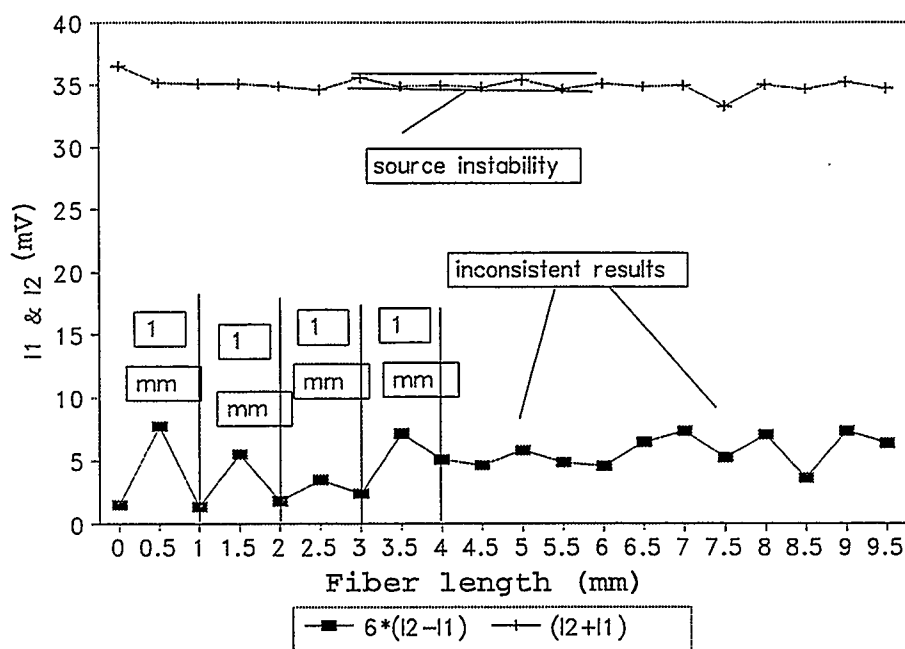


Fig.7.17 Beat lengths measured in F-SPM @ 814nm with (DC) magnetic field.

It can be observed from the figures that the subtraction signal is very small. It is important to appreciate that this is perfectly natural and is due to the weak Faraday effect for the 814 nm wavelength (see Fig.7.10). Finally the fiber F-SPZ is placed in the system to measure its beat length and the results obtained are shown in Figs.(7.18 and 7.19). It can be observed from Figs.(7.12 to 7.19) that the readings are relatively stable and the beat lengths can be easily recognized thus the experimental results are very promising.

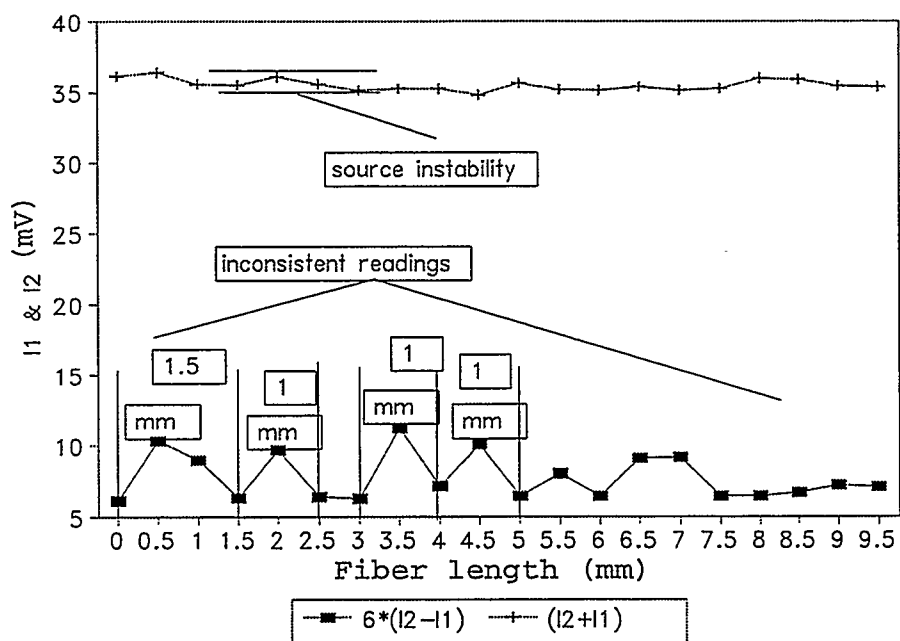


Fig.7.18 Beat lengths measured in F-SPZ @ 814nm with (DC) magnetic field.

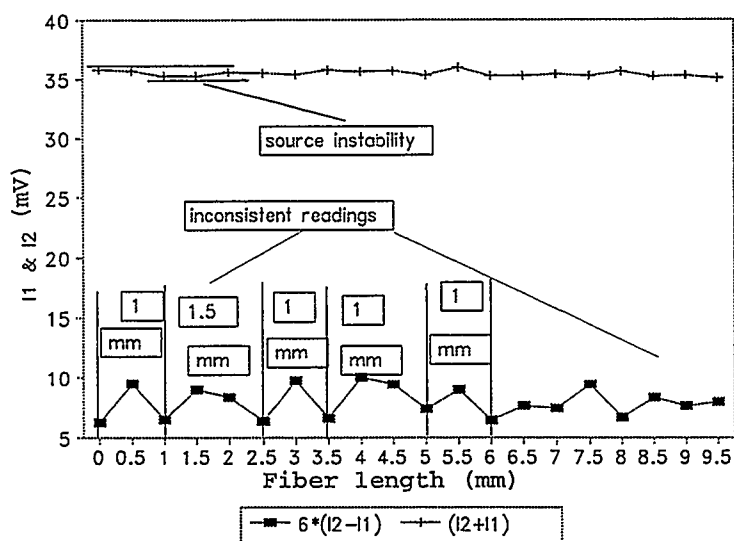


Fig.7.19 Beat lengths measured in F-SPZ @ 814nm with (DC) magnetic field.

7.4 Final results

The results from Figs.(7.12 to 7.19) are relatively acceptable but with a number of inconsistent readings. These results were obtained from a number of sets of readings, that is out of 10 sets of readings, two or three were normally considered acceptable though all sets demonstrated the beat length effect. To obtain even more acceptable results it was decided to introduce further improvements to the system and the system set-up was discussed with a number of experienced persons [30]. Two significant problems areas were identified as a result of these discussions: a) the laser was not mounted on a sufficiently solid stand leading to a significant amount of lateral movement of the beam and b) fiber vibrations. The laser was then mounted on a solid stand and supported at both ends as shown in Fig.7.20.

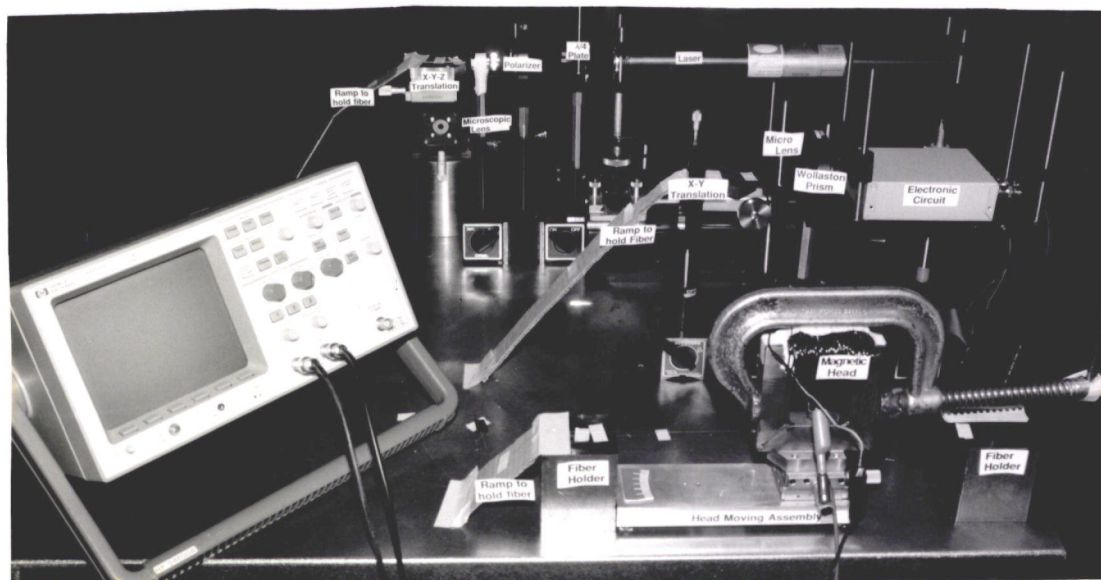


Fig.7.20 The final experimental set-up.

It was also noticed that the fiber mounted on the translation stages was not supported by anything in between. Disturbances in the stretched fiber as a result of air movement or vibration can cause data errors. Hardboard ramps were then installed between the table top and the translation stages and the fiber was laid-down on these ramps and fixed with tape as shown in Fig.7.20.

Implementation of the above procedures introduced very significant improvements in the results such that now out of 10 sets of readings at least 5 to 6 generally give very acceptable results. Figs.(7.21 and 7.22) are the final graphs representing the beat length measurement of Newport's fiber F-SPV. It can be observed from these figures that small beat length can be measured relatively accurately using the proposed method. There are still errors in the curves and these are due to a number of factors to be discussed later. Most of the time the beat length can be read directly from the graph. If this system had a very stable optical output then an averaging of the results at each point along the fiber would probably increase the overall accuracy of the beat length measurement significantly. As a comparison the well known and much used optical time domain reflectometer(OTDR), which is thought of as a very accurate instrument, uses the average of hundreds of samples to arrive at its required value and yet there can be a wide difference in the extremes of the individual values.

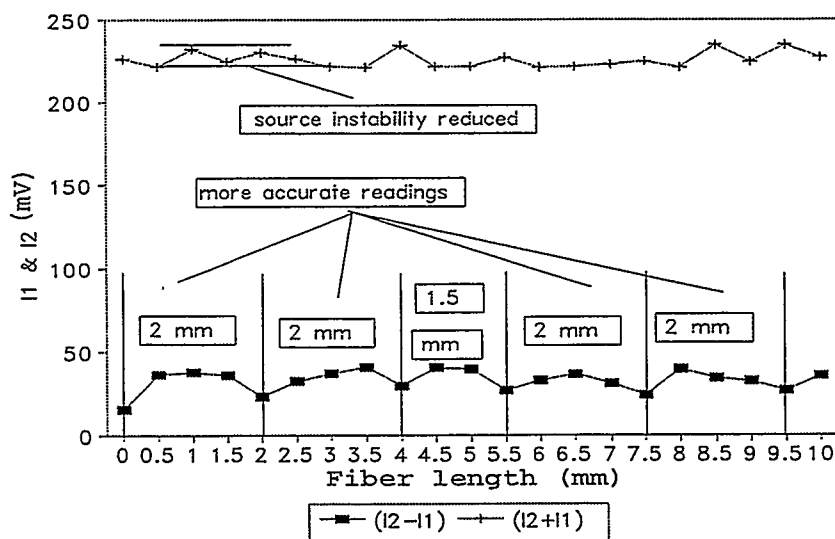


Fig.7.21 Beat lengths measured in F-SPV @ 632nm with (DC) magnetic field.

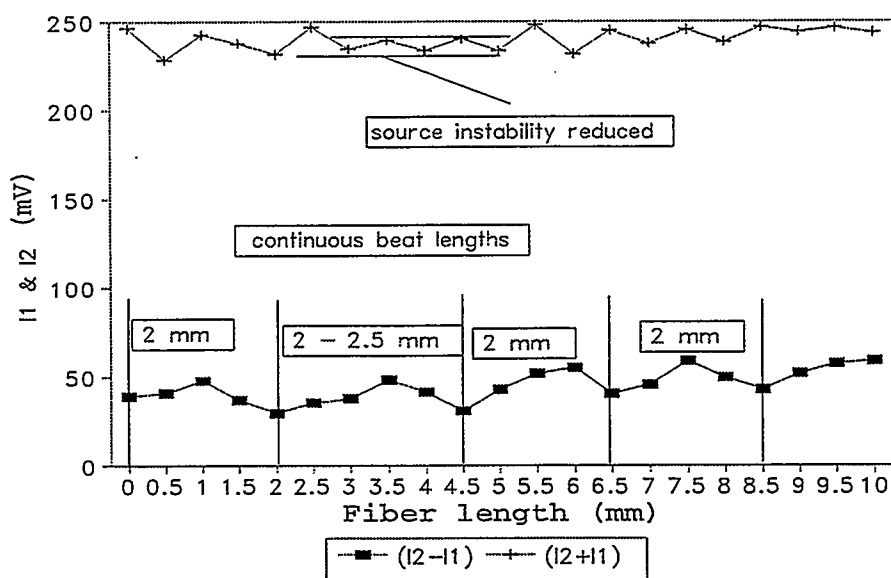


Fig.7.22 Beat lengths measured in F-SPV @ 632 nm with (DC)magnetic field.

Next the fiber F-SPA was placed in the system and the beat length measurements are shown in Figs.(7.23 and 7.24). The fiber F-SPM was then placed in the system and the source changed to the GALA laser diode (814nm). Figs.(7.25 and 7.26) show the beat length measurements for the F-SPM fiber. Again, due to the weaker Faraday effect at 814nm the resultant beam intensities, I_1 and I_2 did not vary greatly but the beat length can still be clearly observed. Since the output power of the GALA laser diode is about 1mW, then the $(I_1 + I_2)$ voltage is at a lower level than with the He-Ne. Figs.(7.27 and 7.28) are for the fiber F-SPZ.

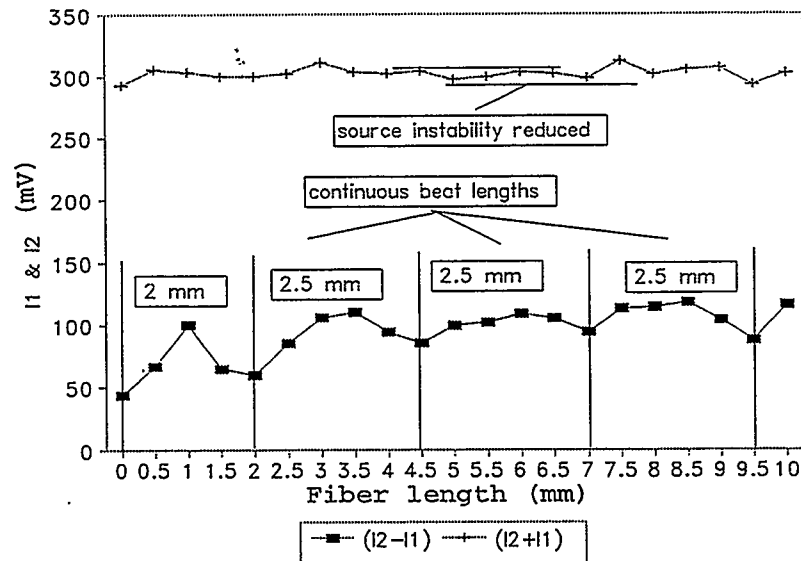


Fig.7.23 Beat lengths measured for F-SPA @ 632nm with (DC) magnetic field.

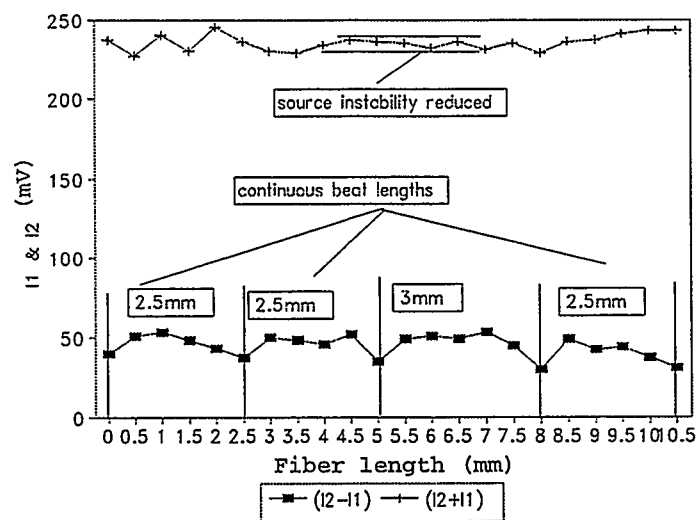


Fig.7.24 Beat lengths measured in F-SPA @ 632nm using (DC) magnetic field.

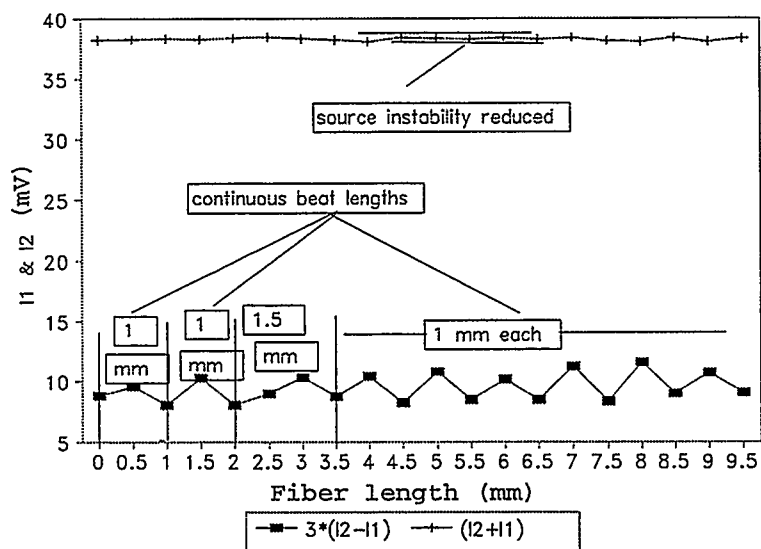


Fig.7.25 Beat lengths measured in F-SPM @ 814nm using (DC) magnetic field.

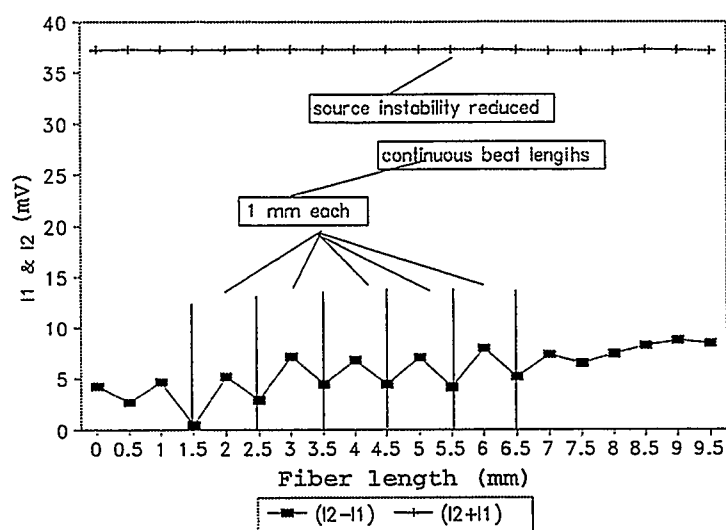


Fig.7.26 Beat lengths measured in F-SPM @ 814nm using (DC) magnetic field.

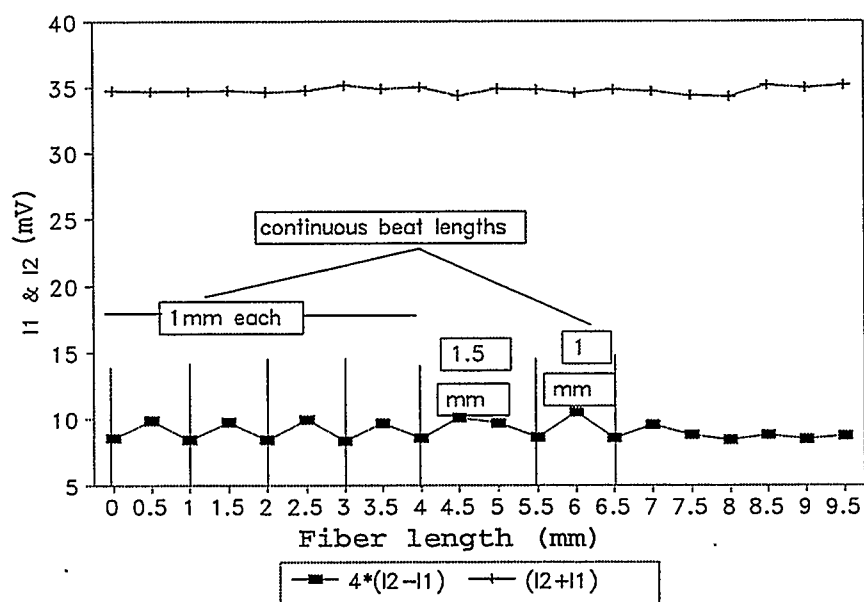


Fig.7.27 Beat lengths measured for F-SPZ @ 814nm using (DC) magnetic field.

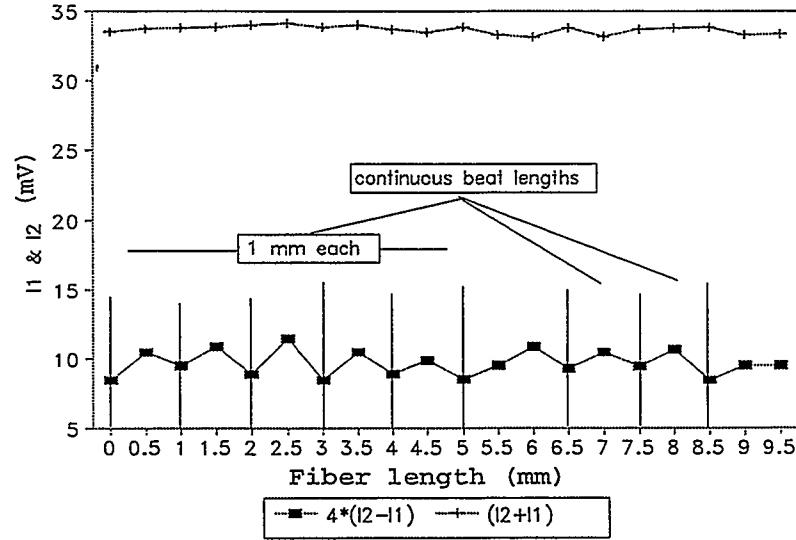


Fig.7.28 Beat lengths measured in F-SPZ @ 814nm using (DC) magnetic field.

Due to moving head assembly limitations the beat lengths of both F-SPZ and F-SPM fibers are measured as 1mm although the given beat lengths were 0.88mm and 1.02mm respectively. As discussed later further improvements can reduce these errors. As a further test of the proposed technique it was decided to measure a fiber at a wavelength for which the beat length had not been provided by the manufacturer. It is known that the beat length is a function of wavelength i.e.

$$\ell_b = \lambda / B_f$$

Thus if the wavelength increases then the beat length increases so the beat lengths of the fibers F-SPV and F-SPA were calculated at the 814nm wavelength of the GALA laser. In

ref.[31], it is stated that the birefringence, B_F , of our tested fibers would be essentially constant over the range of wavelength used.

For the Fiber F-SPV

$$B_F = \lambda / \ell_b = 633 \times 10^{-9} / 2 \times 10^{-3} = 316.5 \times 10^{-6}$$

therefore

$$\ell_b \text{ at } 814\text{nm} = 814 \times 10^{-9} / 316.5 \times 10^{-6} = 2.57\text{mm}.$$

And for fiber F-SPA

$$B_F = \lambda / \ell_b = 514 \times 10^{-9} / 2 \times 10^{-3} = 257 \times 10^{-6}$$

therefore

$$\ell_b \text{ at } 814\text{nm} = 814 \times 10^{-9} / 257 \times 10^{-6} = 3.17\text{mm}.$$

It should be noted that the cutoff wavelengths of the fibers should be less than the operating wavelength or the fiber wills not be single mode. To confirm the above calculated beat lengths the beat lengths of the fibers F-SPV and F-SPA were measured at 814nm. The measured beat lengths for the fiber F-SPV are shown in Figs.(7.29 and 7.30) and for the fiber F-SPA in Figs.(7.31 and 7.32).

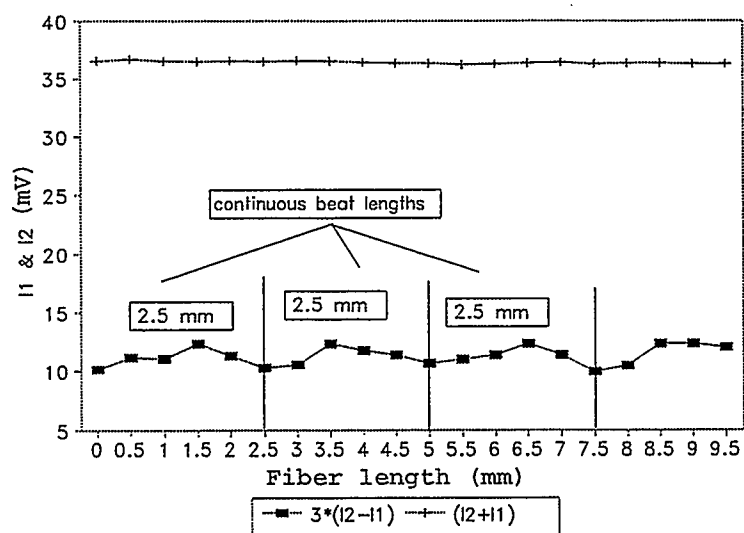


Fig.7.29 Beat lengths measured in F-SPV @ 814nm using (DC) magnetic field.

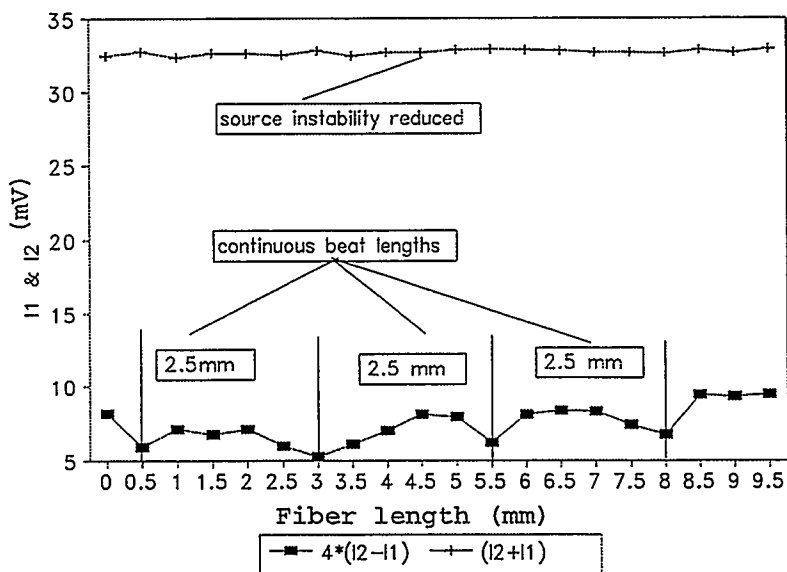


Fig.7.30 Beat lengths measured in F-SPV @ 814nm using (DC) magnetic field.

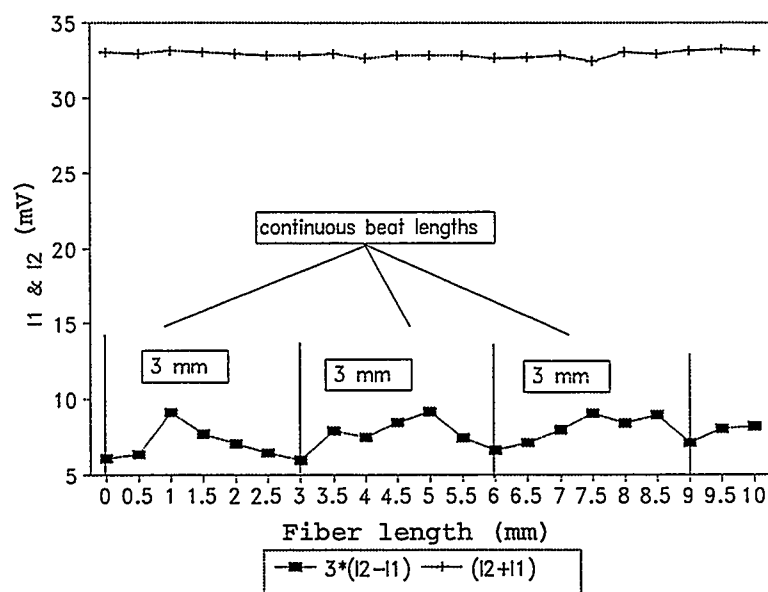


Fig.7.31 Beat lengths measured in F-SPA @ 814nm using (DC) magnetic field.

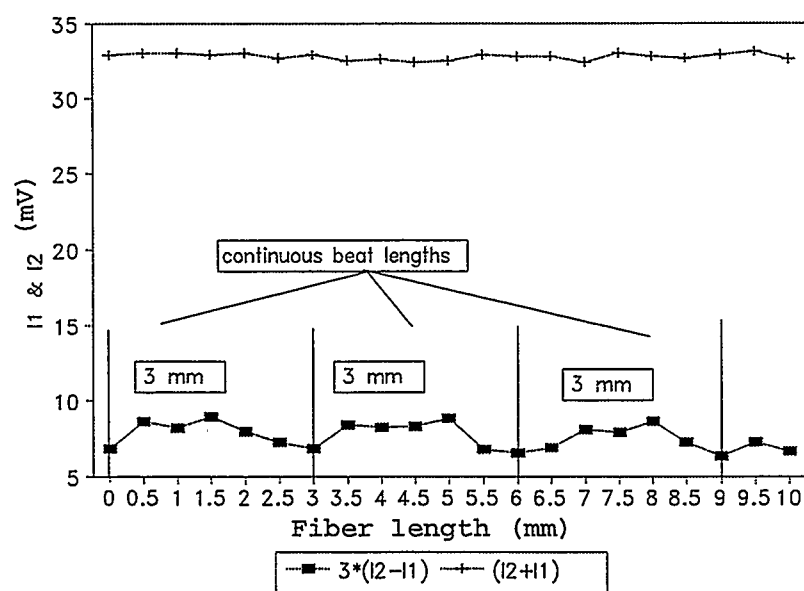


Fig.7.32 Beat lengths measured in F-SPA @ 814nm using magnetic field (DC).

It can be observed from Figs. (7.29 to 7.32) that the measured beat lengths are very close to the calculated values and hence the proposed technique is concluded to have passed the test relatively successfully.

7.5 Analysis of Results

The rectification of the various sources of error in the system has significantly improved the results. The summarized experimental results are shown in Table (7.2) where M.S.V stands for manufacturer supplied value and E.O.V. stands for experimentally obtained value of the beat length.

Table 7.2 Beat length comparisons for the various fibers

	Operating Wavelength 632nm			Operating Wavelength 814nm		
	M.S.V. ℓ_b (mm)	E.O.V. ℓ_b (mm)	% Error	M.S.V. ℓ_b (mm)	E.O.V. ℓ_b (mm)	% Error
F-SPA	2.5	2.5	0	3.17 [#]	3.0	5.6 ^{\$}
F-SPV	2.01	2.0	0.5	2.57 [#]	2.5	2.8 ^{\$}
F-SPZ	@	-	-	0.88	1.0	13.6 ^{\$}
F-SPM	@	-	-	1.02	1.0	2

Notes:

* F-SPV & F-SPA are from Newport.

* F-SPZ & F-SPM are from 3-M.

calculated values

@ The cut-off wavelength is $\geq 700\text{nm}$.

\$ More precise beat length measurement could not be

achieved due to mechanical limitations.

It can be noted from the above table that the maximum error is 13.6%. The error percentage must be viewed in relation to the 0.5mm incremental step size of the head moving assembly though the true error percentage values could be somewhat greater than shown in Table (7.2). The form of experimentally obtained curves would however appear to strongly support the 'proof of concept' nature of this project. The percentage error in the results can be reduced by improving the head moving assembly so the field can be moved smoothly by smaller increments and this could be done by using higher quality precision translation stages. There are still a number of other factors in the system which cause instability in the readings and errors in the results and these are as follows:

a) Noise inherent to photo-detection and signal amplification process. The noise current of the Bi-cell is about 15×10^{-15} A/ $\sqrt{\text{Hz}}$. The noise of the signal processing unit is measured to be about 75 μV . (see Table 6.1). The effect of these noise components can be reduced by using a higher power input signal and that is what we did in this experiment. Increasing the source power may also increase any intensity variation so a laser with a highly stabilized output power will minimize this error.

b) Intensity variations which are due to stray light. These variations are minimized by reducing the ambient light

surrounding the experiment and also by covering the input and output ends of the fiber.

c) Mechanical-optical alignment variations. These variations could be minimized by using precision and stable alignment instruments.

d) Difference in I_1 and I_2 , with no magnetic field, is largely due to electronic component mismatch. Since the dual-path detection scheme has been adopted for this experiment the components for both paths should be virtually identical and this would be practically achieved by using high precision matched components.

The experimental results obtained in our laboratory are very promising and an improved physical set-up can only lead to even better results.

Chapter 8

Conclusion and future work

In this research project, a 'proof of concept' beat length measurement system was developed. The beat lengths of various High Birefringence (Hi-Bi) fibers were measured using the Faraday magneto-optic effect. Experimental procedures and investigations were discussed and successfully conducted.

In light of the literature review the need for this research was discussed. Since the existing techniques have some short-comings such as cutting the fiber during measurement, removing the jacket of the fiber and other physical limitations the proposed technique was implemented. As the Faraday magneto-optic effect is the fundamental basis of this research it was covered in some depth.

With polarized light being used in this research a discussion and mathematical interpretation of polarized light were presented. The structure and operations of the optical components of the system such as the polarizer, lenses and Wollaston prism were discussed in detail and discussion on birefringence were also included. The mechanical components such as the translations stages, component holders and vibration isolated table were also discussed.

Since the magnetic field is a basic component of the

Faraday magneto-optic effect, topics such as electro-magnetism, magnetic cores and cores with air gaps were discussed. The relationship between the air-gap and the beat length was discussed in detail. According to the Faraday magneto-optic effect the Faraday rotation angle is directly proportional to the magnetic field intensity, so a magnetic field intensity of 3000 Gauss was produced in about a millimetre of air-gap this being further increased to 6000 Gauss to enhance the Faraday rotation angle. It was observed that this increase in the magnetic field intensity improved the quality of the experimental results.

In order to obtain acceptable results the following requirements for the light source were fulfilled in this project: a) the input light must be linearly polarized, 2) its power must be sufficient to overcome the noise power of the detection device and the electronic circuit used to measure the Faraday rotation and, c) the wavelength of the light source should fall in the range of large Faraday rotation. To fulfil the above requirements, a) a high quality Glan-Thompson polarizer was used to achieve linearly polarized light, b) a 4 mW He-Ne laser source and a high quality microscope objective lens were used to achieve sufficient power at the output of the single-mode Hi-Bi fiber and, c) most beat lengths were measured at 633nm wavelength for which the Faraday rotation angle is relatively large. A laser diode with an 814nm wavelength was also used to measure the beat lengths

in a number of different fibers in order to extend the scope of the project beyond that achieved by most other researchers to date.

The source intensity variations strongly affected the readings so a division operation $(I_2 - I_1)/(I_2 + I_1)$ was used in an attempt to solve this problem but it was found to be ineffective in this case. A dual path detection and measurement method was used to reduce the source intensity variation effect. Also, noise in the electronic circuit (signal processing unit) was reduced by fabricating it on a printed circuit board and properly shielding it. Shielded cables were used to connect the signal processing unit to the oscilloscope in order to faithfully record the results. Errors in the results due to spurious cladding light in the fiber were eliminated by removing it.

Equipment vibration was a major obstacle in obtaining acceptable results and the critical locations for vibration in the system were the laser (source) holder, the unsupported fiber and the X-Y-Z translation stage at the point of focusing the light into the fiber. These problems were rectified by introducing step-by-step improvements in the set-up such as transferring it to a vibration isolated table and supporting the fiber all the way. It can therefore be concluded from the obtained results that a vibration-isolated system is indeed critical for accurate measurements. The maximum error in the results is 13.6% and this can be reduced by moving the

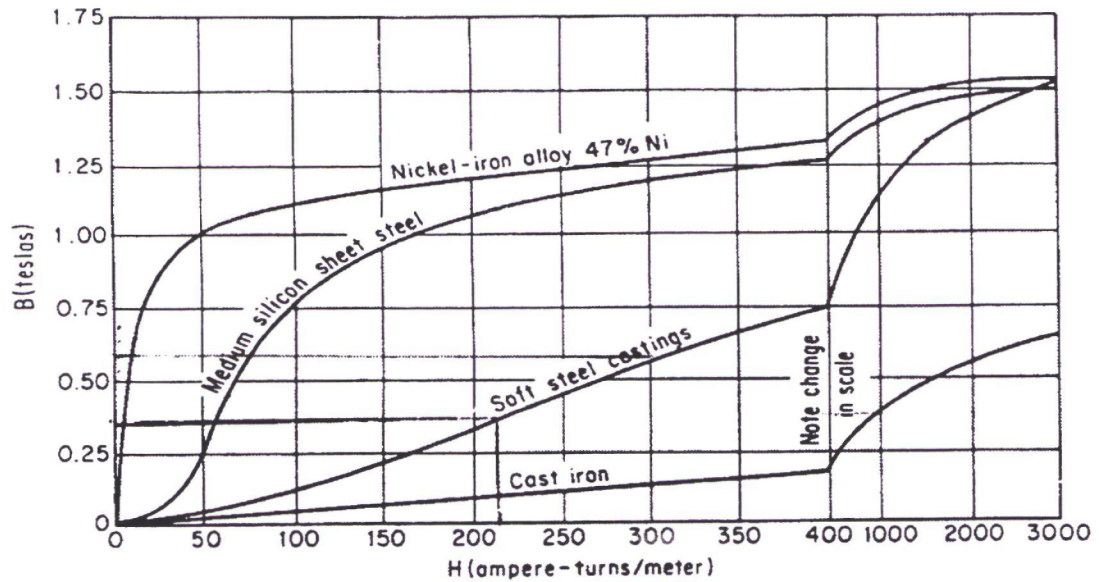
magnetic field along the fiber with an increment of 0.25mm rather than 0.5mm. This could be achieved by improving the moving head assembly.

The experimental studies on the repeatability of the measurement have been carried out and the beat lengths of the four Hi-Bi fibers were successfully measured. Further experiments were also performed to test the technique and it was then successfully used to measure two different beat lengths. So altogether, six beat lengths were measured successfully. Hence the results obtained by this 'proof of concept' technique are very encouraging and it is concluded, with a very high degree of confidence, that the professional development of the proposed set-up would produce excellent results.

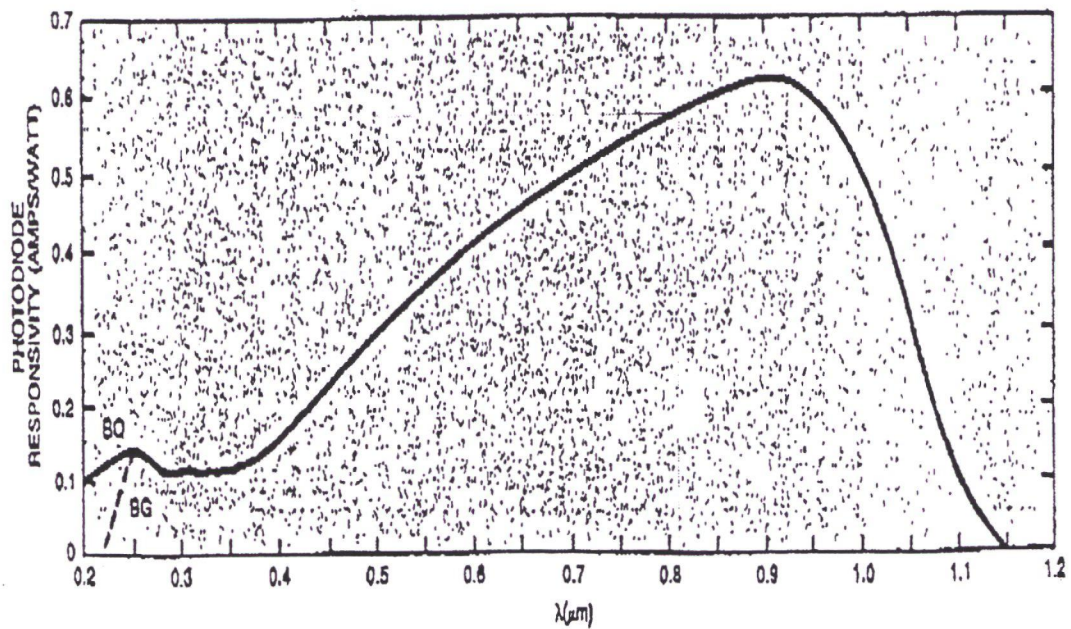
Future work will involve the following tasks:

- a) increasing the magnetic field strength to the allowable extent in order to enhance the Faraday rotation at wavelengths above 820nm.
- b) improving the head moving assembly to increase the measuring limits and enhance measurement accuracy.
- c) improving the source stability.
- d) improving the signal detection and processing circuit capabilities.
- e) reducing vibrations in the system.

Appendices



Magnetization curves of typical Ferromagnetic materials.



Typical Spectral response of Bi-cell (UV-100BG Dual)

Some properties of typical high-coercivity materials

A. Alloys

Material	Chemical composition, wt.% (remainder Fe)	B_R , gs	BH_c , oe	$(BH)_{\max} \cdot 10^6$, gs·oe
Carbon steel	0.65C; 0.85Mn etc.	10 000	42	0.18
” ”	1.00C; 0.50Mn etc.	9 500	51	0.20
Tungsten steel	0.7C; 6W; 0.3Cr; 0.3Mn etc.	10 500	65	0.30
Chrome steel	0.9C; 3.5Cr; 0.4Mn etc.	9 800	70	0.285
Cobalt steel	35Co; 0.9C; 5—6W; 6—3Cr	10 000	250	1.0
Alni	12Al; 25Ni	7 000	500	1.40
Alnico 2	12Al; 18Ni; 13Co; 6Cu	7 300	560	1.70
Magnico	8Al; 13.5Ni; 24Co; 3Cu	13 300	580	4.50
Alnico 5	8Al; 14Ni; 24Co; 3Cu; 0.3Ti	12 700	650	5.50
Ticonal 20	7Al; 15Ni; 34Co; 3Cu; 5Ti	11 800	1315	11.0
Cunife 1	20Ni; 60Cu	5 400	550	1.5
Cunico 2	24Ni; 41Co; 35Cu	5 300	450	1.0
Vicalloy 2	52Co; 13V	10 400	570	4.2
Iron-platinum	77.8Pt	5 830	1570	3.07
” ”	40 Pt	6 000	1900	3.3
Cobalt-platinum	23.3Co; 76.7Pt	4 500	2700	4.0
Platinax 2	50Co; 50Pt	6 400	4800	9.2
MnBi	—	4 300	3400	4.3
SmCo ₅	—	5 780	5130	20.0

B. Ferrites and pressed powders

Material	Chemical composition	B_R , gs	BH_c , oe	$(BH)_{\max} \cdot 10^6$, gs·oe
Cobalt ferrite	CoFe ₂ O ₄	4 000	500	0.95
Barium ferrite (isotropic)	BaO·6Fe ₂ O ₃	2 200	1 850	1.00
Strontium ferrite (textured)	SrO·6Fe ₂ O ₃	4 000	2 200	3.70
Iron powder	Fe	5 700	770	1.60
Iron-cobalt powder	70Fe; 30Co	10 800	980	6.50

References

- [1] J. Noda, K. Okamoto and Y. Sasaki, "Polarization maintaining fibers and their applications," *J. Lightwave Technology.*, vol. LT-4, no. 8, pp.1071-1089, 1986.
- [2] P. G. Zhang and D. Irvine-Halliday, " Measurement of the beat length in Hi-Bi optical fiber by way of magneto-optic modulation," *J. Lightwave Technology.*, vol. 12, no. 4, pp.597-602, 1994.
- [3] M. G. Shlyagin, A. V. Khomenko and D. Tentori, "Birefringence dispersion measurement in optical fibers by wavelength scanning," *Optics Letters*, vol. 20, no. 8, pp. 869-871, 1995.
- [4] Felix P. Kapron, " Birefringence in dielectric optical waveguide," *J. Quantum Electronics.*, vol. QE-8, no. 2, pp.222-225, 1972.
- [5] S. Huang and Z. Lin, "Measuring the birefringence of single-mode fibers with short beat length or non-uniformity: A new Method," *Applied Physics*, Vol.24, no.15, pp. 2355-2361, 1985.
- [6] W. Eickhoff and O. Krumpholz, "Determination of ellipticity of monomode glass fiber for measurement of scattered light intensity," *Electron Letters*, Vol.12, pp.405-405, 1976.
- [7] A. M. Smith, " Polarization and magneto-optic properties

- of single-mode optical fiber," *Applied Optics*, vol. 17, no. 1, pp. 53-56, 1978.
- [8] W.O. Grant, *Understanding light wave transmission*, HBJ Inc; 1988.
- [9] C. Yeh, *Handbook of fiber optics*, Academic Press Inc;1990.
- [10] D. Clark, and J.F. Grainger, *Polarized light and optical measurement*, Pergamon Press, 1971.
- [11] P.S. Hauge, "Techniques of measurement of the polarized altering properties of linear optical system," *SPIE*, Vol.112, pp. 2-11, 1977.
- [12] C. Hentschel, *HP fiber optics handbook*, 2nd ed; 1988.
- [13] Mells-Griot Inc; *Product Handbook*, 1995-1996.
- [14] J. M. Senior, *Optical fiber communications*, 2nd Ed; Prentice Hall Inc; 1992.
- [15] P. B. Ruffin, "Stress and temperature effects on the performance of PM fibers," *SPIE*, Vol.1317, pp. 324-331, 1990.
- [16] R. Passy, A. L. Gama, N. Ginsin and J. Weid; "Pressure dependence of polarization mode dispersion in Hi-Bi fibers," *IEEE Jour. Lightwave Tech*; Vol.10, no. 11, pp. 1527-1531,1992.
- [17] Oriel Corp; *Optics and Filters product handbook*, Vol.III, 1990.
- [18] L. Huang, "Analysis of Wollaston polarizer in imaging

- systems," *SPIE* vol. 1334, pp. 31-42, 1990.
- [19] S. V. Vonsovskii; *Magnetism*, vol.1; John Willey & sons, 1974.
 - [20] V. D. Toro; *Electrical Engineering Fundamentals*, Printice- Hall Inc; N.J; 1972.
 - [21] J. A. Edminister; *Theory and problems of electromagnetics*, 2nd ed; Schaum outlines series, McGraw Hill Inc; 1993.
 - [22] M. J. Freiser, "A survey of Magneto-optic effects," *IEEE Trans. on Magnetism*, Vol. MAG-4, No.2. pp. 152-161, 1968.
 - [23] F. A. Jenkins, H. E. White, *Fundamentals of optics*, 4th ed. McGraw Hill, 1976.
 - [24] P-G. Zhang, " *Faraday Effect Optical Current Sensor*," Master's thesis, University of Calgary, 1994.
 - [25] G. Liu, B. Wu, " Magneto-optic effects of solids and their properties," *ACTA Optica Sinica*, vol. 8, pp. 105-115, Feb.1988.
 - [26] R. C. Jones; " A new calculus for the treatment of the optical systems, part I-III", *J. Opt. Soc. Am*; vol.31, pp. 488-503, 1941.
 - [27] A. M. Smith; " Optical fibers for current measurement applications," *Optics and Laser Technology*, pp 25-29. Feb.1980.
 - [28] M. Born; and E. Wolf; *Principles of optics*, Oxford: Pergamon, 1968.

- [29] Newport Canada Inc; Product literature.
- [30] D. Clegg; *TR labs*, Edmonton.
- [31] D. Payne, A. J. Barlow and J. Hansen, " Development of low and high-birefringence optical fibers," *J. Quantum Electronics.*, vol.QE-18, no.4, pp.477-487, 1982.